


2015

The interaction mechanisms of a screw dislocation with a defective coherent twin boundary in copper

Qiongjiali Fang
University of Vermont

Follow this and additional works at: <https://scholarworks.uvm.edu/graddis>

 Part of the [Condensed Matter Physics Commons](#), [Mechanics of Materials Commons](#), and the [Nanoscience and Nanotechnology Commons](#)

Recommended Citation

Fang, Qiongjiali, "The interaction mechanisms of a screw dislocation with a defective coherent twin boundary in copper" (2015).
Graduate College Dissertations and Theses. 457.
<https://scholarworks.uvm.edu/graddis/457>

This Thesis is brought to you for free and open access by the Dissertations and Theses at ScholarWorks @ UVM. It has been accepted for inclusion in Graduate College Dissertations and Theses by an authorized administrator of ScholarWorks @ UVM. For more information, please contact donna.omalley@uvm.edu.

THE INTERACTION MECHANISMS OF A SCREW DISLOCATION WITH A
DEFECTIVE COHERENT TWIN BOUNDARY IN COPPER

A Thesis Presented

by

Qiongjiali Fang

to

The Faculty of the Graduate College

of

The University of Vermont

In Partial Fulfillment of the Requirements
for the Degree of Master of Science
Specializing in Mechanical Engineering

October, 2015

Defense Date: August 27, 2015
Thesis Examination Committee:

Frederic Sansoz, Ph.D., Advisor
Ting Tan, Ph.D., Chairperson
Jianing Li, Ph.D.

Cynthia J. Forehand, Ph.D., Dean of the Graduate College

ABSTRACT

$\Sigma 3\{111\}$ coherent twin boundary (CTB) in face-centered-cubic (FCC) metals and alloys have been regarded as an efficient way to simultaneously increase strength and ductility at the nanoscale. Extensive study of dislocation-CTB interaction has been carried out by a combination of computer simulations, experiments and continuum theory. Most of them, however, are based on the perfect CTB assumption. A recent study [Wang YM, Sansoz F, LaGrange T, et al. Defective twin boundaries in nanotwinned metals. *Nat Mater.* 2013;12(8):697-702.] has revealed the existence of intrinsic kink-like defects in CTBs of nanotwinned copper through nanodiffraction mapping technique, and has confirmed the effect of these defects on deformation mechanisms and mechanical behavior. One of the deformation mechanisms proposed therein, i.e. general hard dislocation slip intersecting with kink line is studied here in detail by molecular dynamics (MD) simulation. Simulations are performed using copper bicrystal models with a particular focus on the interaction of a screw dislocation with 0 degree and 60 degree kinked CTBs. It is found that kink-like defects have a profound impact on screw dislocation - CTB interaction mechanisms, resulting in significant strengthening or softening effects.

ACKNOWLEDGEMENTS

First and foremost, I would like to thank my advisor, Dr. Frederic Sansoz for accepting me into his group, providing me with an interesting thesis topic to work on, and for his guidance and support during the last two years. I am thankful for the helpful suggestions provided by the other members of my thesis committee, Dr. Jianing Li and Dr. Ting Tan. I would also like to acknowledge my current and former labmates, Erin, Dan, Aaron, Ryan, Cory, Xing and Rodrigo for a warm and friendly lab environment. Lastly, I would also like to thank my family and friends for their encouragement along the way.

This work was made possible through the computational resources provided by Extreme Science and Engineering Discovery Environment (XSEDE) supported by National Science Foundation (NSF) grant number ACI-1053575 and Vermont Advanced Computing Core supported by NASA (NNX-08AO96G). Support from NSF grant DMR-1410646 and teaching assistantship from the University of Vermont are also gratefully acknowledged.

TABLE OF CONTENTS

	Page
ACKNOWLEDGEMENTS.....	ii
TABLE OF CONTENTS.....	iii
LIST OF TABLES.....	v
LIST OF FIGURES	vi
CHAPTER 1: INTRODUCTION.....	1
CHAPTER 2: METHODOLOGY	5
2.1. Molecular Dynamics.....	5
2.1.1. Embedded atom method potential	6
2.1.2. velocity-Verlet algorithm.....	8
2.2. Visualization and analysis	9
2.2.1. Common neighborhood analysis	9
2.2.2. Dislocation extraction analysis	11
2.2.3. Atomic strain	12
2.2.4. The concept of virial stress and von-Mises stress	13
2.3. Implemented model	15
2.3.1. Screw dislocation.....	16
2.3.2. Coherent twin boundary	16
2.3.3. Kink-like twin boundary defect	17
2.3.4. Full MD Model	18
2.3.5. Constant shear strain.....	20

CHAPTER 3: PERFECT COHERENT TWIN BOUNDARY	21
3.1. Interaction mechanisms	21
3.2. Generalized stacking/twinning fault energy curves.....	27
CHAPTER 4: COHERENT TWIN BOUNDARY WITH KINK-LIKE DEFECT	31
4.1. Influence of kink-like defect on interaction mechanism	31
4.1.1. 0 degree kink.....	31
4.1.2. 60 degree kink.....	38
4.1.3. Summary.....	44
4.2. Influence of kink-like defect on the mechanical behavior.....	46
CHAPTER 5: CONCLUSIONS	52
References.....	55

LIST OF TABLES

Table	Page
Table 1. Interaction mechanism between screw dislocation and perfect/0 degree kinked/60 degree kinked coherent twin boundaries under various shear strains.....	45
Table 2. Linear fit trend line slope after 7.6 ps in different models and a comparison with the case of perfect CTB under shear strain of 0.80%.	47
Table 3. Linear fit trend line slope after 7.6 ps in different models and a comparison with the case of perfect CTB under shear strain of 1.21%.	48
Table 4. Linear fit trend line slope after 7.6 ps in different models and a comparison with the case of perfect CTB under shear strain of 2.01%.	49
Table 5. Linear fit trend line slope after 7.6 ps in different models and a comparison with the case without CTB under shear strain of 2.41%.	50
Table 6. Linear fit trend line slope after 7.6 ps in different models and a comparison with the case of perfect CTB under shear strain of 2.81%.	51

LIST OF FIGURES

Figure	Page
Figure 1. (a) TEM images of as-deposited Cu samples with mean twin thicknesses of 4 nm; (b) Uniaxial tensile true stress–true strain curves for nt-Cu samples tested at a strain rate of $6 \times 10^{-3} \text{ s}^{-1}$ with mean twin thickness varying from 4 nm to 96 nm, a twin-free sample with a mean grain size of 500 nm (ufg) and 10 μm (cg).[3]	2
Figure 2. (a) Edge-on high-resolution IPFOM image of CTBs; (b) MD model with kinked CTB. (GB – grain boundary, CTB – coherent twin boundary.) Some selected kinks are marked with white arrows.[19]	3
Figure 3. Illustration of CNA of (a) FCC atomic structure; (b)(c) HCP atomic structures.	10
Figure 4. (a) The Burgers circuit method in a continuum setting and in an atomistic crystal; (b) Illustration of sweeping process to find dislocation line.[29]	11
Figure 5. Schematic illustration of MD method used to create a screw dislocation intersecting a CTB.	15
Figure 6. (a) Coherent twin boundary and stacking sequence; (b) Staking of atoms above CTB; (c) Staking of atoms below CTB.	17
Figure 7. (a)(b) Topology analysis of two possible ITB structure;[36] (c)(d) Atomic structure of ITB corresponding to (a)(b); Thompson tetrahedron illustration of interaction of screw dislocation with (e) 0 degree kinked CTB (kink is at distance x to the dislocation) and (f) 60 degree kinked CTB.	18

Figure 8. Full MD model. (a) Screw dislocation and perfect coherent twin boundary; (b) Screw dislocation and 0 degree kinked coherent twin boundary ($x=7.06$ nm); (c) Screw dislocation and 0 degree kinked coherent twin boundary ($x=3.08$ nm); (d) Screw dislocation and 0 degree kinked coherent twin boundary ($x=0$ nm); (e) Screw dislocation and 60 degree kinked coherent twin boundary; (f) Viewing angle for results in Chapter 4..... 19

Figure 9. Left side view of the model (a) before (b) after constant shear strain..... 20

Figure 10. Interaction of screw dislocation with perfect CTB under shear strain of 0.80%. (a) CNA at 3.6 ps; (b) CNA at 6.8 ps, dissociated screw dislocation combine into a full dislocation at CTB; (c) CNA at 9.6 ps, full dislocation re-dissociate into two partial dislocations on CTB; (d) Atomic strain at 9.6 ps. This mechanism is referred to as Mechanism D..... 24

Figure 11. Interaction of screw dislocation with perfect CTB under shear strain of 1.21%. (a) CNA at 3.6 ps; (b) CNA at 6 ps, dissociated screw dislocation combine into a full dislocation at CTB; (c) CNA at 9.6 ps, full dislocation penetrates CTB, and becomes two partial dislocations in twin grain; (d) Atomic strain at 9.6 ps. This mechanism is referred to as Mechanism T. 25

Figure 12. Interaction of screw dislocation with perfect CTB under shear strain of 2.41%. (a) CNA at 3.6 ps; (b) CNA at 5.2 ps, dissociated screw dislocation combine into a full dislocation at CTB; (c) CNA at 9.6 ps, there is one partial dislocation on CTB and another partial dislocation in twin grain connected by a stair-rod dislocation at CTB; (d) Atomic strain at 9.6 ps. This mechanism is referred to as Mechanism L. 26

Figure 13. Model for calculating generalized stacking/twinning fault energy curve. (a) Single crystal; (b) After rigid displacement in single crystal, a stacking fault is generated; (c) Staking sequence before (upper) and after (lower) rigid displacement in

single crystal; (d) Bi-crystal separated by coherent twin boundary; (e) After rigid displacement, coherent twin boundary moves up by one atomic layer; (f) Staking sequence before (upper) and after (lower) rigid displacement in bi-crystal.	28
Figure 14. Generalized stacking/twinning fault energy curves.	29
Figure 15. Interaction of screw dislocation with 0 degree kinked ($x=3.08$ nm) CTB under shear strain of 2.41%. (a) CNA at 0 ps; (b) CNA at 4.2 ps, dissociated screw dislocation combine into a full dislocation at CTB; (c) CNA at 7.6 ps, full dislocation becomes one partial on CTB and one partial in twin grain connected by a stair-rod dislocation at CTB; (d) atomic strain at 7.6 ps; (e) CNA at 11.6 ps, the partial dislocation and stair-rod dislocation on CTB re-combine into another partial dislocation which transmits to the twin grain; (f) atomic strain at 11.6 ps.	32
Figure 16. Interaction of screw dislocation with 0 degree kinked ($x=0$ nm) coherent twin boundary under shear strain of 0.80%. (a) CNA at 5.6 ps, screw dislocation recombines at twin boundary; (b) CNA at 7.6 ps, three partial dislocations are generated on twin boundary; (c) CNA at 11.6 ps, partial dislocation 1 moves in one direction, while partial dislocation 2 and 3 move in another direction; (d) Atomic strain at 11.6 ps. This mechanism is referred to as Mechanism D'.	33
Figure 17. Interaction of screw dislocation with 0 degree kinked ($x=0$ nm) coherent twin boundary under shear strain of 2.41%. (a) CNA at 4.4 ps; (b) CNA at 7.6 ps, three partial dislocations are generated on twin boundary; (c) CNA at 11.6 ps, three partial dislocations moves in the same direction; (d) atomic strain at 11.6 ps. This mechanism is referred to as Mechanism D''.	34
Figure 18. Thompson tetrahedron illustration of interaction mechanisms between screw dislocation and 0 degree kinked CTB. Burgers vectors of partial dislocations (a) before interaction; (b-c) after interaction.	36

Figure 19. Interaction of screw dislocation with 0 degree kinked ($x=0$ nm) CTB under shear strain of 3.62%. (a) CNA at 4.4 ps, kink moves upwards under shear strain, steps are formed in kink ; (b) CNA at 5.6 ps, screw dislocation transmits into the twin grain; (c) CNA at 7.6 ps; (d) Atomic strain at 7.6 ps; (e) CNA at 11.6 ps, steps on kink disappear; (f) Atomic strain at 11.6 ps..... 37

Figure 20. Interaction of screw dislocation with 60 degree kinked coherent twin boundary under shear strain of 0.80%. (a) CNA at 0 ps; (b) CNA at 6.4 ps; (c) CNA at 8.4 ps;; (d) CNA at 10 ps; (e) DXA at 6.4 ps. 39

Figure 21. Interaction of screw dislocation with 60 degree kinked coherent twin boundary under shear strain of 1.21%. (a) CNA at 0 ps; (b) CNA at 11.6 ps; (c) CNA at 17.2 ps; (d) CNA at 19.6 ps. 40

Figure 22. Interaction of screw dislocation with 60 degree kinked coherent twin boundary under shear strain of 2.01%. (a) CNA at 0 ps; (b) CNA at 7.6 ps; (c) CNA at 11.6 ps; (d) A schematic illustration of screw dislocation intersecting with twin boundary on different plane. 41

Figure 23. Interaction of screw dislocation with 60 degree kinked coherent twin boundary under shear strain of 2.41%. (a) CNA at 0 ps; (b) CNA at 7.6 ps; (c) CNA at 8.8 ps; (d) CNA at 11.6 ps. Yellow arrow indicates the partial emitted from kink. 42

Figure 24. Interaction of screw dislocation with 60 degree kinked coherent twin boundary under shear strain of 2.81%. (a) CNA at 0 ps; (b) CNA at 6 ps; (c) CNA at 8.4 ps; (d) CNA at 11.6 ps. 43

Figure 25. DXA of interaction of screw dislocation with 60 degree kinked coherent twin boundary under shear strain of 2.81%. 44

Figure 26. Variation of von-Mises stress over time under shear strain of 0.80%. 46

Figure 27. Variation of von-Mises stress over time under shear strain of 1.21%.	47
Figure 28. Variation of von-Mises stress over time under shear strain of 2.01%.	49
Figure 29. Variation of von-Mises stress over time under shear strain of 2.41%.	50
Figure 30. Variation of von-Mises stress over time under shear strain of 2.81%.	51

CHAPTER 1: INTRODUCTION

Strengthening of materials has been a popular research topic ever since the last century. Four traditional strengthening mechanisms - grain size refinement, solid solution alloying, precipitation strengthening and work hardening – has already been widely applied in industry.[1] With the development in nanotechnology, one new strategy to produce ultrastrong metal is introduced by decreasing the grain size into nanometer regime. The strengthening effect of this strategy originates from the well-known Hall-Petch relation: plastic deformation is more difficult at smaller grain size since grain boundaries can block the motion of lattice dislocation.

Two major drawbacks, however, has hindered the application of this new strategy in engineering. First, as the grain size decreases, the high excess energy from grain boundaries becomes so large that grains would grow easily even at ambient temperature or below. Second, strong as it is, these nanograined metals become extremely brittle even if their coarse-grained forms are very ductile.[2]

$\Sigma 3\{111\}$ coherent twin boundary (CTB) in face-centered-cubic (FCC) metals and alloys at the nanoscale is found to be an efficient way to simultaneously increase strength and ductility. Lu et al.[3,4] have shown that ultrafine grained Cu with CTB with mean twin thickness of 15 nm could achieve ultrahigh strength of 1 GPa and high ductility of 14% elongation to failure.

Moreover, CTBs can be generated favorably in FCC metals with low stacking fault energies by crystal growth, phase transformation, plastic deformation or

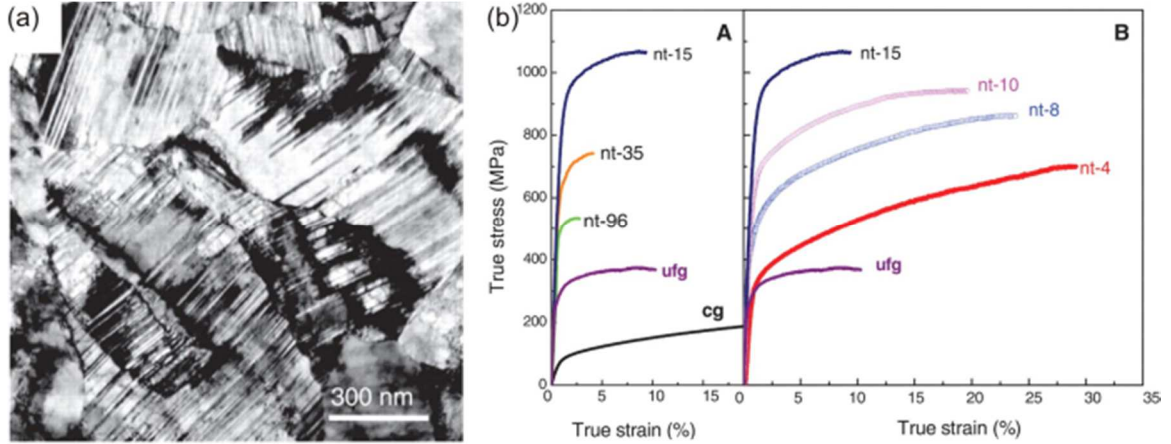


Figure 1. (a) TEM images of as-deposited Cu samples with mean twin thicknesses of 4 nm; (b) Uniaxial tensile true stress–true strain curves for nt-Cu samples tested at a strain rate of $6 \times 10^{-3} \text{ s}^{-1}$ with mean twin thickness varying from 4 nm to 96 nm, a twin-free sample with a mean grain size of 500 nm (ufg) and 10 μm (cg).[3]

recrystallization. [5,6] In addition, the low excess energy of CTBs (one order of magnitude lower than that of grain boundaries) makes them much more stable against migration, which is a fundamental process of coarsening. CTB also has higher thermal, lower electrical resistivity and better corrosion resistance.[7,8]

In order to understand the effect of twin boundaries on the mechanical behavior of metal, extensive study on nanotwinned system has been obtained from a combination of experiments, computer simulation and continuum theory in the past several year. Using molecular dynamics (MD) simulations, Jin et al.[9,10] studied the interaction of dislocation with CTB by bicrystal model in Cu, Ni, and Al. These authors concluded that the interaction mechanism depends on the dislocation type (screw/non-screw), stress and the material. Also Deng and Sansoz investigated by MD the effects of twin boundary on the mechanical behavior of nanowires.[11,12] They found that near ideal strength can be achieved in gold nanowires by a combined design of surface morphology and twin size. Furthermore, Wu et al.[13] performed MD simulations of the CTB-dislocation

interaction mechanisms and size scale effect in more realistic three-dimensional microstructures, while the synthetic effect of twin size and grain size in polycrystalline nanotwinned metals was simulated by Li et al.[14] Molecular statics simulation was applied by Chassagne et al.[15] to study the interaction of screw dislocation with CTB. Atomic reaction pathway was modeled to investigate the effects of temperature and strain rate on plastic yielding of nanotwinned system on the time scale of laboratory experiment.[16,17] Zhu et al.[18] provided a systematical description of all plausible dislocation-CTB interaction mechanisms.

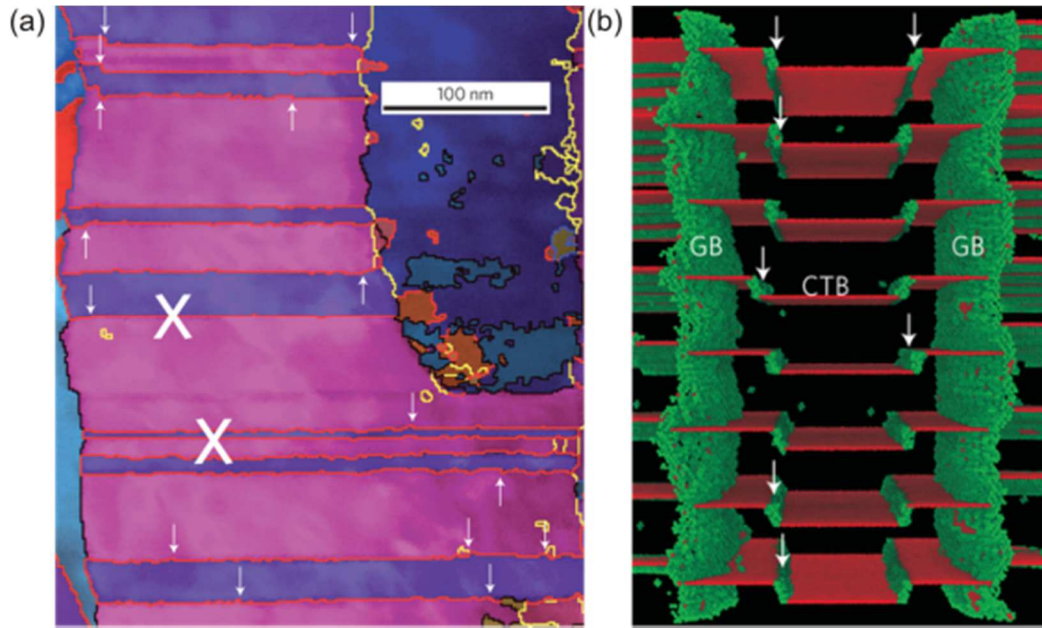


Figure 2. (a) Edge-on high-resolution IPFOM image of CTBs; (b) MD model with kinked CTB. (GB – grain boundary, CTB – coherent twin boundary.) Some selected kinks are marked with white arrows.[19]

These computational and theoretical studies have underscored the unique role of CTBs in nanotwinned metals, and all these models are assuming the CTBs to be interfaces with perfect lattice matching. A recent study by Wang and Sansoz et al.[19], however, found the existence of intrinsic kink-like defects, which are indeed a very tiny

segment of $\Sigma 3(112)$ incoherent twin boundary (ITB) in CTB in nanotwinned (nt) copper through nanodiffraction mapping technique as shown in Figure 2(a). It was confirmed that these defects played a crucial role in the deformation mechanisms and mechanical behavior. MD simulation in this research indicates that there could be unknown kink-dependent deformation processes that differ from conventional mechanisms in nt metals with perfect CTBs. Possible mechanisms include: general hard slip intersecting kink line, pinning of threading dislocations intersecting kink lines, dislocation nucleation from kink-GB intersection, kink motion, kink emitting twinning partial dislocations parallel to twin boundaries.

The primary objective of this thesis is to conduct a detailed study of the general hard slip intersecting a kink-like defect in a CTB by using MD simulation, with particular focus on the screw dislocation (Burgers vector parallel to the dislocation line) in copper. Computational methodology and the implemented model are presented in Chapter 2. Chapter 3 presents the deformation mechanisms associated with a screw dislocation intersecting with a perfect CTB. Chapter 4 shows the results for kinked CTBs, and discusses the strengthening versus softening effects resulting from either perfect or kinked CTBs. The major conclusions of this thesis are summarized in Chapter 5.

CHAPTER 2: METHODOLOGY

2.1. Molecular Dynamics

With the development of the first sufficiently powerful computers, computer simulation techniques like Monte Carlo (MC) and Molecular Dynamics (MD) were developed for the first time in 1950s. Molecular dynamics (MD) is a scientific tool that models atom or molecular interactions from approximations of real physical or chemical system. The principles of such “virtual experiment” was first envisioned and applied in theoretical physics by Alder and Wainwright in late 1950s where only several hundred of classical elastic spheres were studied.[20,21]

MD is now a mature and powerful research tool that has been applied in materials science, biological systems, molecular physics and chemistry. The rapid development in this technique has benefited a lot from the rapid evolution in high performance computing. The work by Alder and Wainwright can now be carried out on personal computers. Larger calculations which needs to take multi CPU months or years can also be completed in hours or days by parallel computation, which decompose the MD simulation into smaller units and spread them out to individual nodes. The availability of MD software packages specializing in a variety of areas has made it even more attractive.

In this study, MD simulations are performed using Large-scale Atomic/Molecular Massively Parallel Simulator (LAMMPS)[22] developed by Sandia National Laboratories. Most of the calculations are performed on SuperMIC, a supercomputer part of the XSEDE research network. The system is simulated under microcanonical ensemble, i.e. NVE ensemble (atom number, volume and energy of the system are kept

as constant). The initial temperature is set to be 0.1 K in order to avoid thermal activated dislocation cross slip in the process.

In the MD framework, each atom or molecule is represented as a point of mass in space, particles move due to forces acting on them as described by Newton's second law of motion:

$$\vec{F} = m\vec{a} = m\vec{v}' = \vec{p}' = m\vec{r}'' \quad (1)$$

Here, F is the force acting on the particle, p is the momentum, m is the mass of the particle, v is the velocity, a is the acceleration, and r is the position of the particle, prime and double prime indicates first and second order derivative over time respectively. In order to find the trajectory of the particles, a potential function is needed to find the forces on each particle and a numerical integration technique is required to evaluate the motion of the particles.

2.1.1. Embedded atom method potential

Potential energy functions play a significant role in MD simulations, since the force on each atom is found by taking the space derivative of the potential energy:

$$\vec{F} = -\nabla U(\vec{r}_1, \vec{r}_2, \dots, \vec{r}_N) \quad (2)$$

The potential function $U(\vec{r}_1, \vec{r}_2, \dots, \vec{r}_N)$ describes how the potential energy of a system of N atoms depends on the coordinates of the atoms $(\vec{r}_1, \vec{r}_2, \dots, \vec{r}_N)$. Potential functions include (with an increasing level of complexity and accuracy) empirical potential (e.g. Lennard-Jones, Morse), semi-empirical potential (e.g. Embedded Atom potential, Glue Model), and direct quantum-mechanics-based potential (so-called *ab-initio* MD simulation). In this study, Embedded Atom Method (EAM) potential, a type

of semi-empirical potential, is applied. EAM potential has been proved to provide useful results in face-centered-cubic metallic system, while not being too computationally expensive.

The total energy of a system with N atoms can be described by an empirical potential as a summation of one body term, two body term (pair term) and three body term, etc.

$$U(\vec{r}_1, \vec{r}_1, \dots, \vec{r}_1) = \sum_{i=1}^N U_1(r_i) + \frac{1}{2} \sum_{i=1}^N \sum_{\substack{j=1 \\ j \neq i}}^N U_2(\vec{r}_i, \vec{r}_j) + \frac{1}{6} \sum_{i=1}^N \sum_{\substack{j=1 \\ j \neq i}}^N \sum_{\substack{k=1 \\ k \neq i \\ k \neq j}}^N U_3(\vec{r}_i, \vec{r}_j, \vec{r}_k) + \dots \quad (3)$$

Based on this expansion, semi-empirical potentials can be divided into two classes: pair potentials (only U_2 is present) and many body potentials (U_3 and higher terms are included). Pair potentials, however, cannot provide an adequate description of metallic systems. EAM is a kind of pair-functional potential based on pair potential, but its correction based on the concept of the local density to pair potential allows one to describe the bonding in metallic system.

$$E_i = F_i(\rho_i) + \frac{1}{2} \sum_{j \neq i} \phi_{ij}(r_{ij}), \text{ where } \rho_i = \sum_{j \neq i} f_j(r_{ij}) \quad (4)$$

The potential energy of atom i defined in EAM is given by E_i in Equation (4). In this equation, the embedding function F finds the energy associated with placing atom i in its surrounding the electron environment ρ_i , while the pair potential term ϕ describes electrostatic contributions. Function f describes the distribution to the electronic density at the site of atom i from atom j , the sum over function f therefore determines ρ_i , the local electron density at the position of the atom i . Only atoms within a cut-off distance are

considered in this calculation to reduce simulation time. The EAM potential used in this study is developed by Mishin et al.[23], this potential was chosen since it is calibrated according to the *ab initio* values of stacking fault and twin formation energies.

2.1.2. velocity-Verlet algorithm

Forces find from potential energy must be integrated to find the trajectory of particles in MD. Since MD system can include millions of particles, it is impossible to solve analytically. Therefore, numerical integration method is applied. Numerical integration techniques include Verlet algorithm, leap-frog algorithm, velocity-Verlet, and Beeman's algorithm, etc.

In molecular dynamics, the most commonly used time integration algorithm is Verlet algorithm. The basic idea is to write two third-order Taylor expansions for the position $r(t)$, one forward and one backward in time:

$$r(t + \Delta t) = r(t) + v(t)\Delta t + \frac{1}{2}a(t)\Delta t^2 + \frac{1}{6}b(t)\Delta t^3 + O(\Delta t^4) \quad (5)$$

$$r(t - \Delta t) = r(t) - v(t)\Delta t + \frac{1}{2}a(t)\Delta t^2 - \frac{1}{6}b(t)\Delta t^3 + O(\Delta t^4) \quad (6)$$

Here, v is the velocity, a is the acceleration, and b is the third derivatives of r with respect to t , adding the two expressions gives:

$$r(t + \Delta t) = 2r(t) - r(t - \Delta t) + a(t)\Delta t^2 + O(\Delta t^4) \quad (7)$$

This method is very accurate since the truncation error of the algorithm is the order of Δt^4 . Velocity can be calculated from the positions by using

$$v(t) = \frac{r(t+\Delta t) - r(t-\Delta t)}{2\Delta t} \quad (8)$$

The error associated to this expression, however, is of order Δt^3 . To overcome this drawback, some variants of the verlet algorithm have been developed. The molecular dynamics software applied in this thesis, LAMMPS, uses velocity-Verlet integration, where positions, velocities and accelerations at time $t + \Delta t$ are obtained from the same quantities at time t in the following way:

$$r(t + \Delta t) = r(t) + v(t)\Delta t + \frac{1}{2}a(t)\Delta t^2 \quad (9)$$

$$v\left(t + \frac{\Delta t}{2}\right) = v(t) + \frac{1}{2}a(t)\Delta t \quad (10)$$

$$a(t + \Delta t) = -\frac{1}{m}\nabla V(r(t + \Delta t)) \quad (11)$$

$$r(t + \Delta t) = v\left(t + \frac{\Delta t}{2}\right) + \frac{a(t+\Delta t)}{2}\Delta t \quad (12)$$

Timestep Δt is generally on the order of femtoseconds to avoid discretization errors. In the application of this thesis, the timestep was chosen to be two femtosecond.

2.2. Visualization and analysis

2.2.1. Common neighborhood analysis

In order to analyze the deformed crystal structure, relevant information needs to be extracted from the numerical coordinates output from MD simulations, which is not very illuminating itself. Method regularly used to recognize defect (dislocations, boundaries, point defects, etc.) include energy or stress filtering, atomic local shear strain tensor coloring, coordination number (CN), bond angle analysis (BAA), central symmetry parameter (CSP), common neighbor analysis (CNA), voronoi analysis (VA), etc. CNA proposed by Honeycutt and Andersen[24] is applied here.

CNA finds the local crystal structure of atoms using topology of bonds that connect the surrounding neighbor. A set of four indexes: i, j, k and l are used. If a pair of atoms, α and β are near-neighbors, then $i = 1$, otherwise, $i = 2$. The number of near-neighbors shared by α and β (i.e. the common neighbors) is represented by the second index, j . The third index, k , indicates the number of bonds between these common neighbors. The fourth index, l , differentiates diagram with the same i, j , and k indexes and different bonding between the common neighbors.[25,26]

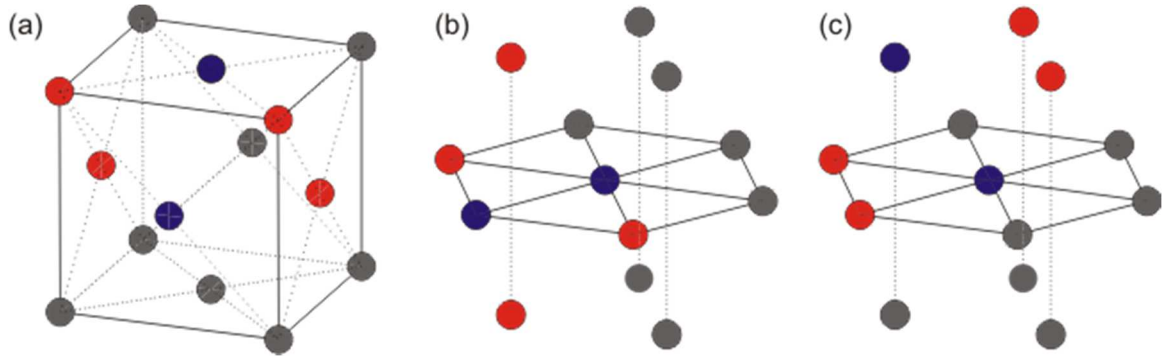


Figure 3. Illustration of CNA of (a) FCC atomic structure; (b)(c) HCP atomic structures.

Figure 3 presents topology in the FCC and HCP (hexagonal close packed) structure. One pair of nearest neighbors is colored blue, and their common nearest neighbors are colored red. Both FCC and HCP have four common nearest neighbors, hence $j = 4$. These four neighbors all have two bonds, hence $k = 2$. For HCP, the bonding between these four atoms have two possibilities as shown in Figure 3(b) and 3(c), the indexes of them are 1421 and 1422. FCC has only one set of index 1421. In HCP structure half the pairs of nearest neighbor atoms form 1421 while the other half form 1422. CNA in LAMMPS encode FCC, HCP and unknown atoms as integer values 1, 2 and 5 respectively. OVITO was used for visualization[27], which colored FCC, HCP and unknown atoms to be blue, light blue and red respectively.

2.2.2. Dislocation extraction analysis

Although CNA and other methods listed in 2.2.1 can detect defects, a common weakness in them is that they provide no information on the type of crystal defect the atoms form. Researchers have to guess which defect structures constitute dislocation lines base on theory and experience. A new computer code, Crystal Analysis Tool (CAT)[28], developed by Alexander Stukowski at Technische Universitat Darmstadt, Germany has made it possible to find the Burgers vector of dislocation lines by implementing Dislocation Extraction Algorithm (DXA)[29]. This program is a very convenient post-processing tool since can automatically detect and read the atomic coordinates written in dump files from LAMMPS and other MD programs.

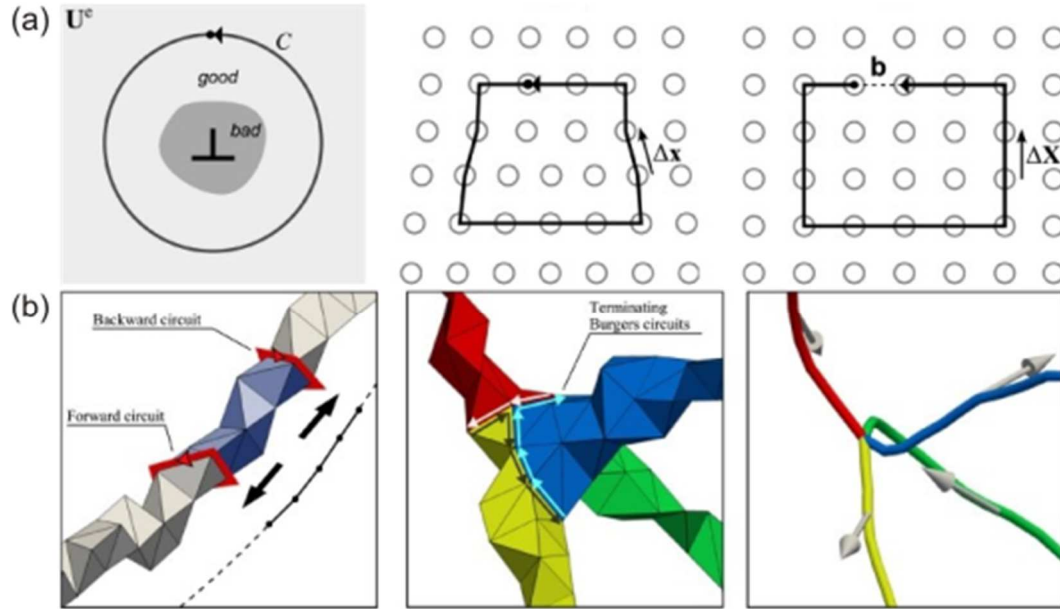


Figure 4. (a) The Burgers circuit method in a continuum setting and in an atomistic crystal; (b) Illustration of sweeping process to find dislocation line.[29]

CAT first analyze the local structure by CNA. It then partitions the system into clusters via a pattern matching algorithm trying to match every atom to ideal structure templates, like perfect lattice, stacking fault, CSL grain boundaries, etc. Elastic

deformation gradient field will then be found based on a Delaunay mesh generated with tetrahedral elements each connecting four close atoms. If a dislocation is present, it will be multi-valued depending on the three edges picked out of the six possible edges of the tetrahedron, and these multivalued elements will be classified as bad ones. A boundary surface that separates the good tetrahedral from bad tetrahedron will then be generated.

Closed circuits of increasing length are generated on the interface mesh until a first circuit with a non-zero Burgers vector is found. This non-zero burgers vector is then duplicated and reversed, and advanced along the interface mesh in both directions. A one-dimensional line representation of the center of pass of dislocation segment will be generated. This process is repeated until the entire interface mesh has been scanned for circuits on its surface with non-zero Burgers vector content and all dislocation segments in the crystal are discovered. Dislocation junctions can be identified by detecting collisions of multiple circuits on the interface mesh.[29] OVITO[27] can be utilized for visualization.

2.2.3. Atomic strain

To quantify plastic deformation at the atomic level and to identify the dislocation movement path, the atomic local shear strain η_i^{Mises} for each atom i [30,31] will be calculated and visualized by OVITO[27].

Atomic strain first calculates the local deformation gradient tensor for each particle from the relative displacement of the particle's neighbors within the given cutoff radius. Calculation of atomic strain η_i^{Mises} requires two atomic configurations, one current $\{\mathbf{x}_i\}$, and one reference $\{\mathbf{x}_i^0\}$ (superscript 0 means the reference configuration).

For each neighbor j of atom i , their current separation vector is

$$\mathbf{d}_{ji} = \mathbf{x}_j - \mathbf{x}_i \quad (13)$$

and their reference separation vector is

$$\mathbf{d}_{ji}^0 = \mathbf{x}_j^0 - \mathbf{x}_i^0 \quad (14)$$

The local transformation matrix \mathbf{J}_i , is found from the best map of $\{\mathbf{d}_{ji}^0\} \rightarrow \{\mathbf{d}_{ji}\}, \forall j \in N_i^0$. \mathbf{J}_i is determined by minimizing

$$\sum_{j \in N_i^0} |\mathbf{d}_{ji}^0 \mathbf{J}_i - \mathbf{d}_{ji}|^2 \rightarrow \mathbf{J}_i = (\sum_{j \in N_i^0} \mathbf{d}_{ji}^{0T} \mathbf{d}_{ji}^0)^{-1} (\sum_{j \in N_i^0} \mathbf{d}_{ji}^{0T} \mathbf{d}_{ji}) \quad (15)$$

Here N_i^0 is the total number of nearest neighbors of atom i at the reference configuration. For each \mathbf{J}_i , the local Lagrangian strain matrix is computed

$$\boldsymbol{\eta}_i = \frac{1}{2} (\mathbf{J}_i \mathbf{J}_i^T - \mathbf{I}) \quad (15)$$

Local von-Mises shear invariant of atom i can be calculated as

$$\eta_i^{Mises} = \sqrt{\eta_{xy}^2 + \eta_{xz}^2 + \eta_{yz}^2 + \frac{(\eta_{xx} - \eta_{yy})^2}{6} + \frac{(\eta_{xx} - \eta_{zz})^2}{6} + \frac{(\eta_{yy} - \eta_{zz})^2}{6}} \quad (16)$$

2.2.4. The concept of virial stress and von-Mises stress

To determine the mechanical property of a material, one need to find the stress field in it. Since stress is inherently a continuum concept, it is difficult to define in physically reasonable manner at the atomic scale. A lot of research has been carried out too develop the proper definition of continuum variables that are calculable within an atomic system, and they are usually developed using balance equations and long-wavelength (long-time) averages. The equivalent atomic stress used in this study is the

virial stress, which is based on a generalization of the virial theorem of Clausius for gas pressure[32]. It includes two parts expressed as:

$$\sigma_{ij}^V = \frac{1}{V} \sum_{\alpha} (R_i^{\beta} - R_i^{\alpha}) F_j^{\alpha\beta} - m^{\alpha} v_i^{\alpha} v_j^{\alpha} \quad (17)$$

where (i, j) is the direction (x, y or z), β is a variable from 1 to N neighbors of atom α , R is the position of atom along direction i , F is the force along direction j on atom α to atom β , V is the total volume, m is the mass of atom α , and v is the thermal excitation velocity of atom α . [33]

There is a controversy about virial stress ever since Zhou et al.[34] brought up that virial stress cannot be regarded as an equivalence to Cauchy stress as it violates the classical conservation of linear momentum, and only the potential part of virial stress should be included to find mechanical stress.

Nevertheless, Dommelen[35] has proved some of Zhou's examples are flawed. In this work the original formula is maintained since the initial temperature of the system is 0.1 K, and the increase in temperature due to released elastic energy is less than 5 K.

In the application of LAMMPS, atomic stress is calculated for each atom, their six stress components are added up, and then divided by the total volume of the model. In order to study the strengthening or softening effect, von-Mises stress is calculated from the virial stress.

$$\sigma^{Mises} = \sqrt{\frac{1}{2} [(\sigma_{xx}^2 + \sigma_{yy}^2 + \sigma_{zz}^2) + \frac{1}{6} (\sigma_{xy}^2 + \sigma_{xz}^2 + \sigma_{yz}^2)]} \quad (18)$$

2.3. Implemented model

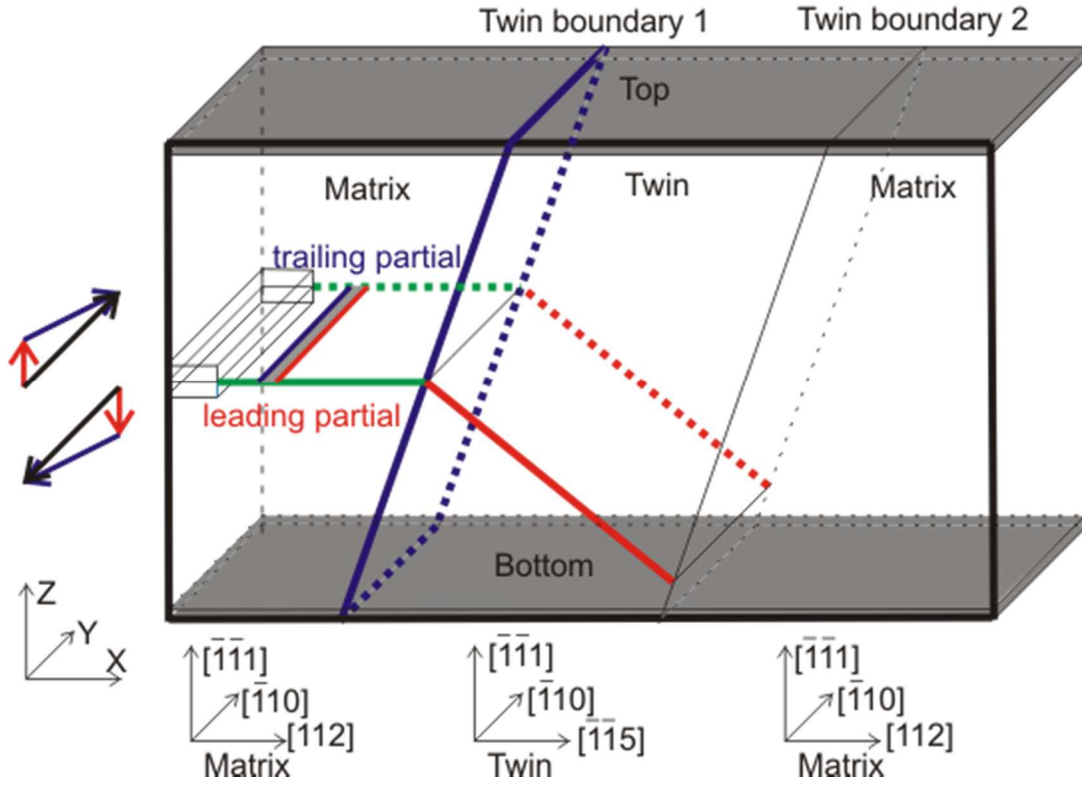


Figure 5. Schematic illustration of MD method used to create a screw dislocation intersecting a CTB.

MD cell as shown in Figure 5 has a dimension of $L_x = 50 * a_0 * \sqrt{6}$, $L_y = 3 * a_0 * \sqrt{2}$ and $L_z = 40 * a_0 * \sqrt{3}$, where a_0 is the lattice parameter of copper (3.085 Å). The whole cell consisted of about 150,000 atoms. Periodic boundary conditions (PBC) were applied in x and y directions. This model was applied to study perfect twin boundary and 0 degree kinked twin boundary, larger model in y direction would not affect the results. Dimension in y direction was increased to $20L_y$ in the study of 60 degree kinked CTB in order to realize the geometry.

2.3.1. Screw dislocation

In order to study the interaction of screw dislocation with twin boundary, a single screw dislocation was introduced in the matrix on the left side of the model. Method similar to the one used by Jin et al.[9] is applied here. The boundary condition in x direction was free in Jin's model, but was considered periodic here. Hence, instead of applying a linearly decreasing rigid displacement to all atoms in the leftmost 10 layers of atoms in the model, a constant rigid displacement was applied to 12 layers of atoms in the middle of this 10 left most layers as shown in Figure 1. The upper 6 layers and lower 6 layers were displaced by the same distance in opposite directions as shown by black arrows on its left in two steps. The first relative displacement was $a_0\sqrt{6}/6$ toward the $[2\bar{1}1]$ direction (red arrow); the second $a_0\sqrt{6}/6$ toward $[1\bar{2}\bar{1}]$ direction (blue arrow). Displacements of all the atoms in that 12 layers were strictly confined within the horizontal planes. After such rigid displacement, a dissociated screw dislocation with a stacking fault ribbon (about 11 Å) connecting the leading and trailing Shockley partials was automatically formed.

2.3.2. Coherent twin boundary

A CTB is a special type of grain boundary with perfect mirror symmetry across the interface. The stacking sequence on either side of the CTB (light blue) is opposite to each other, as shown in Figure 6(a). Above CTB, the stacking sequence is ABCABC, atoms in the top layer lies in the downward triangle formed by the atoms in the bottom layer; Below CTB, the stacking sequence is CBACBA, atoms in the upper layer lies in the upward triangle formed by atoms in the lower layer. Two twin boundaries are

introduced in this bicrystal model in order to achieve periodic boundary condition in x direction. The lattice orientation of the twin and matrix are shown in Figure 5.

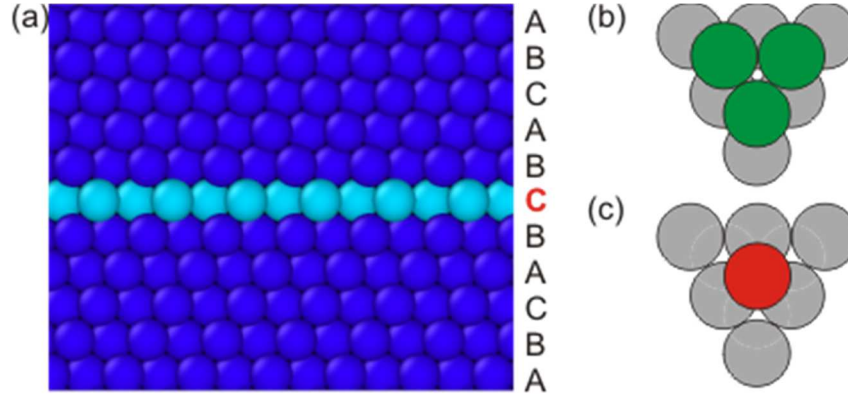


Figure 6. (a) Coherent twin boundary and stacking sequence; (b) Staking of atoms above CTB; (c) Staking of atoms below CTB.

2.3.3. Kink-like twin boundary defect

Topological analysis by Wang et al.[36] shows that $\Sigma 3\{112\}$ ITBs have two types of atomic structure with different arrangement of Shockley partial dislocations as shown in Figure 7(a) and 7(b). Four layers of atoms will form a smallest unit of ITB, and the Burgers vector of the Shockley partials in it adds up to zero. Figure 7(c) and 7(d) are the respective atomistic model of this smallest unit. The current study will focus kink-like structure in Figure 7(c).

Since dislocation will become parallel to twin boundary before intersection due to image force, screw dislocation can only interact with the kink-like defect from two different directions as shown in Figure 7(e) and 7(f). The screw dislocation line can either be parallel to the kink or at a 60 degree angle to the kink. For the parallel case, the distance from screw dislocation to the kink (x) could be different.

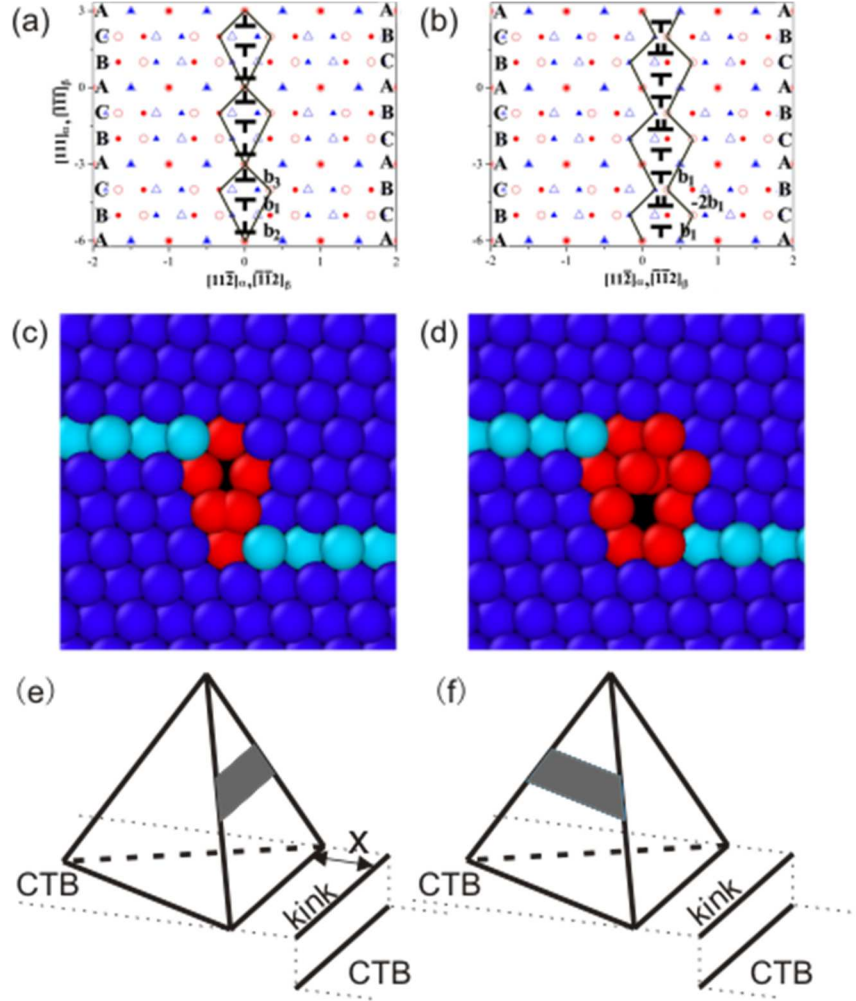


Figure 7. (a)(b) Topology analysis of two possible ITB structure;[36] (c)(d) Atomic structure of ITB corresponding to (a)(b); Thompson tetrahedron illustration of interaction of screw dislocation with (e) 0 degree kinked CTB (kink is at distance x to the dislocation) and (f) 60 degree kinked CTB.

2.3.4. Full MD Model

Figure 8 presents the full atomic models applied in this research. Figure 8(a) shows the model for the screw dislocation - perfect CTB intersection. The results obtained from this model are presented in Chapter 3. Figure 8(b-d) represents the model for a screw dislocation intersecting a CTB containing a 0 degree kink located at a distance x equal to 7.06 nm, 3.08 nm, and 0 nm respectively. Figure 8(e) shows the 60 degree kink

model, two kinks are introduced in order to maintain the periodic boundary condition in y direction. The view angles shown in Figure 8(f) is applied to get snapshots. Results for both 0 degree and 60 degree kink are presented in Chapter 4.

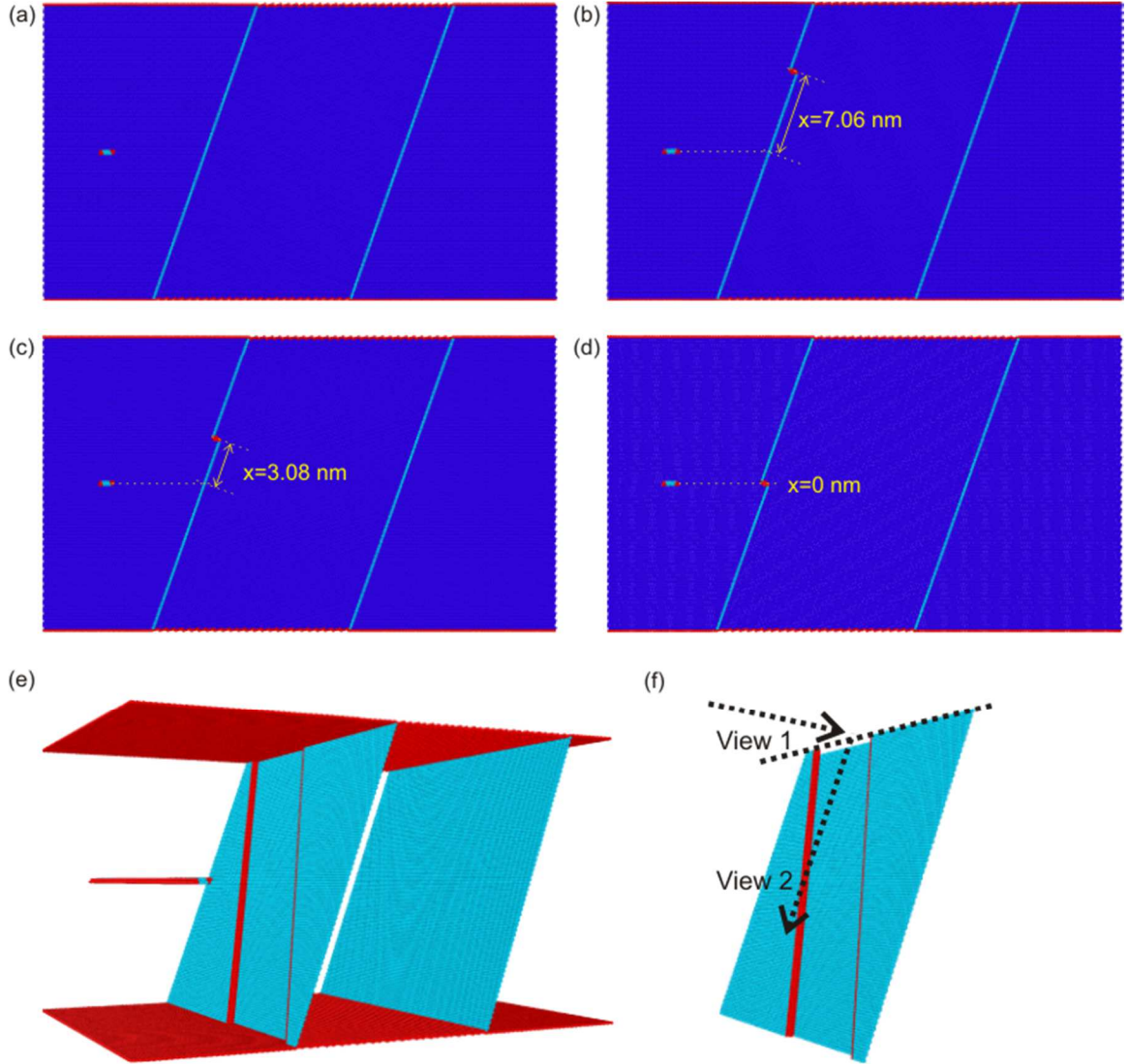


Figure 8. Full MD model. (a) Screw dislocation and perfect coherent twin boundary; (b) Screw dislocation and 0 degree kinked coherent twin boundary ($x=7.06$ nm); (c) Screw dislocation and 0 degree kinked coherent twin boundary ($x=3.08$ nm); (d) Screw dislocation and 0 degree kinked coherent twin boundary ($x=0$ nm); (e) Screw dislocation and 60 degree kinked coherent twin boundary; (f) Viewing angle for results in Chapter 4.

2.3.5. Constant shear strain

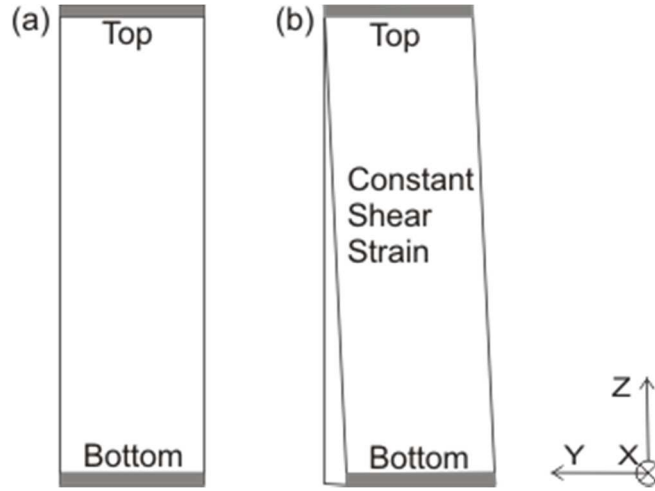


Figure 9. Left side view of the model (a) before (b) after constant shear strain.

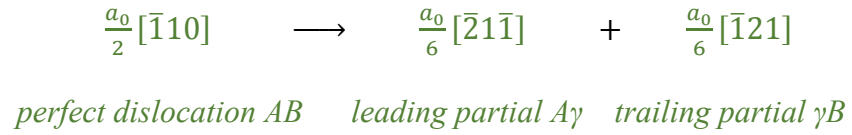
After introducing the screw dislocation, CTB and kink-like defects, the energy of the model was minimized using conjugate gradient method. A constant shear strain was then applied to the model as shown in Figure 9. Figure 9(a) is the left side view of the model before shear, a displacement linearly increasing from 0 to the desired value was applied to the whole model from the bottom to the top as shown in Figure 9(b). In order to keep this constant strain, three layers of atoms at the top and bottom (grey color) were fixed in subsequent MD runs. After the constant shear strain was applied, the model was allowed to relax. To study the influence of applied shear stress on the interaction mechanisms, different shear strains were applied to the model. With rigid displacement of top layer 2 Å, 3 Å, 4 Å, 5 Å, 6 Å and 7 Å, the simulated shear strain was 0.80%, 1.21%, 1.61%, 2.01%, 2.41%, 2.81% respectively.

CHAPTER 3: PERFECT COHERENT TWIN BOUNDARY

3.1. Interaction mechanisms

The interaction between screw dislocation and perfect CTB has been studied by others by MD[9], molecular statics[15], and atomistic reaction pathway[17]. Two different mechanisms were found depending on the material and applied shear strain. In this study, however, another mechanism that is less understood before was also predicted.

In FCC metals, full dislocation would dissociate into two Shockley partials connected by a stacking fault according to



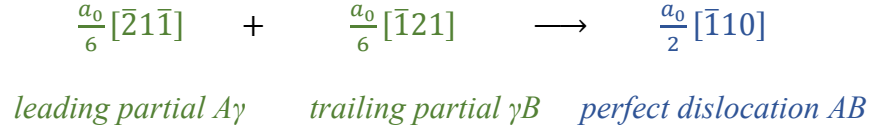
This reaction is energetically favorable according to Frank's rule ($\frac{a_0^2}{2} > \frac{a_0^2}{6} + \frac{a_0^2}{6}$). The color of the Burgers vectors in the equation is in accordance with the color of their slip planes shown in Figure 5.

Under applied shear strain ε_{yz} , screw dislocation would move toward the CTB during relaxation. Three different shear strain condition 0.80%, 1.21%, 2.41% is discussed here to illustrate three different interaction mechanisms between screw dislocation and perfect CTB, which is shown in Figure 10, Figure 11 Figure 12 respectively. Time in the figures all starts from relaxation. To have a better view, the figures are all zoomed into the area near intersection point.

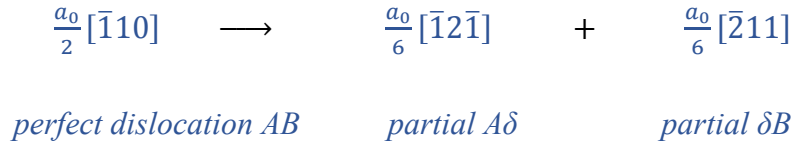
Figure 10(a), 11(a) and 12(a) are the CNA at 3.6ps, the distance from the leading partial to the twin boundary is 3.52 nm, 2.97 nm and 2.08 nm respectively (before

relaxation, the distance is 7.87 nm), which correspond to an average dislocation movement speed of 1208.3 m/s, 1361.11 m/s and 1608.3 m/s.

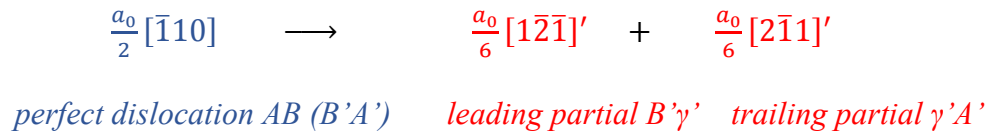
Figure 10(b), 11(b) and 12(b) are the CNA at 6.8 ps, 6 ps and 5.2 ps, when leading partial and trailing partial recombine into a full dislocation at CTB. After that, the full dislocation choose to dissociate at different path depending on the applied shear strain.



Under the lowest shear strain 0.80%, full dislocation dissociated into two partial dislocations moving in different directions along CTB as shown by the CNA and atomic strain in Figure 10(c) and 10(d). This mechanism is referred to as Mechanism D (Dissociation) in the following context. It can be expressed by:

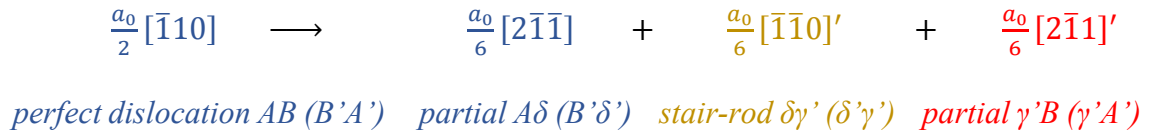


Under the medium shear strain 1.21%, full dislocation transmitted through the CTB, and re-dissociated into two partial dislocations on a slip plane in the twin grain. The CNA and atomic strain at 9.6 ps are shown in Figure 11(c) and 11(d) respectively. Atomic strain indicates that the slip plane before and after interaction are mirror symmetric across the CTB. This mechanism is referred to as Mechanism T (Transmission) in the following context, and can be expressed by:

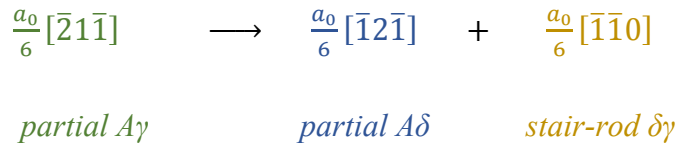


The prime indicates that the vector is defined in the twin grain coordinate system.

Under high shear strain 2.41%, a less understood mechanism is observed. The recombined full dislocation becomes one partial on the CTB and one partial in the twin grain, which are connected by a stair-rod dislocation at the exact location of the full dislocation before dissociation. The stair-rod dislocation wouldn't move since it is a sessile dislocation, this kind of structure is named Lomer-lock. This mechanism is referred to as Mechanism L (Lomer-lock) in the following context, it can be expressed by:



Lomer-locks were reported by Afanasyev and Sansoz[37] in twinned nanowires. In their study, the leading partial is dissociated into a stair-rod and a partial dislocation on the CTB,



the trailing partial is left behind in the matrix grain, and a Lomer dislocation is formed by these three dislocations. As the trailing partial is forced into the CTB, the Lomer dislocation is unlocked. The Lomer-lock here, however, is formed after leading and trailing partial combined to a full dislocation, one partial and one stair-rod are on CTB, and another partial is in the twin grain.

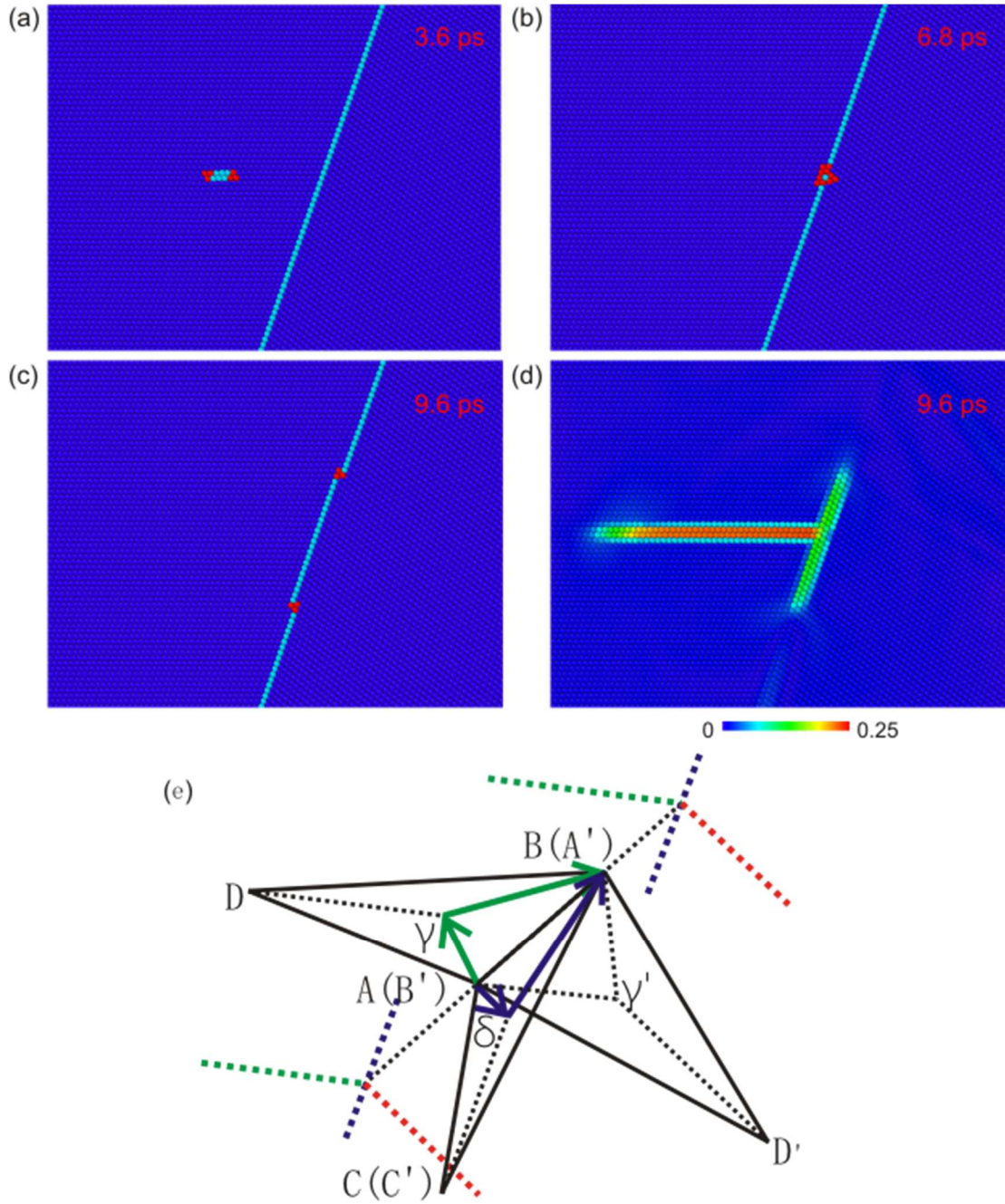


Figure 10. Interaction of screw dislocation with perfect CTB under shear strain of 0.80%. (a) CNA at 3.6 ps; (b) CNA at 6.8 ps, dissociated screw dislocation combine into a full dislocation at CTB; (c) CNA at 9.6 ps, full dislocation re-dissociate into two partial dislocations on CTB; (d) Atomic strain at 9.6 ps. This mechanism is referred to as Mechanism D.

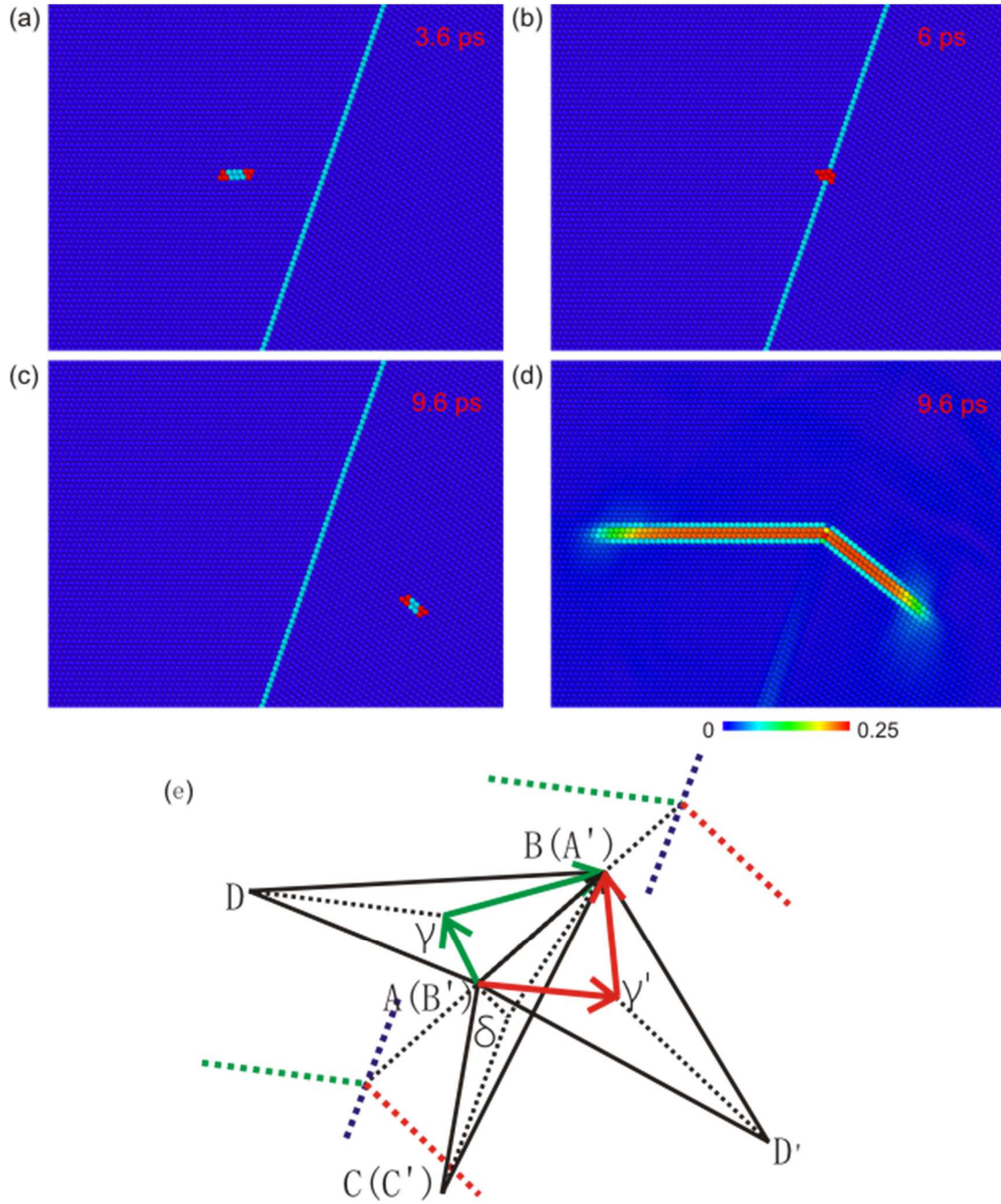


Figure 11. Interaction of screw dislocation with perfect CTB under shear strain of 1.21%. (a) CNA at 3.6 ps; (b) CNA at 6 ps, dissociated screw dislocation combine into a full dislocation at CTB; (c) CNA at 9.6 ps, full dislocation penetrates CTB, and becomes two partial dislocations in twin grain; (d) Atomic strain at 9.6 ps. This mechanism is referred to as Mechanism T.

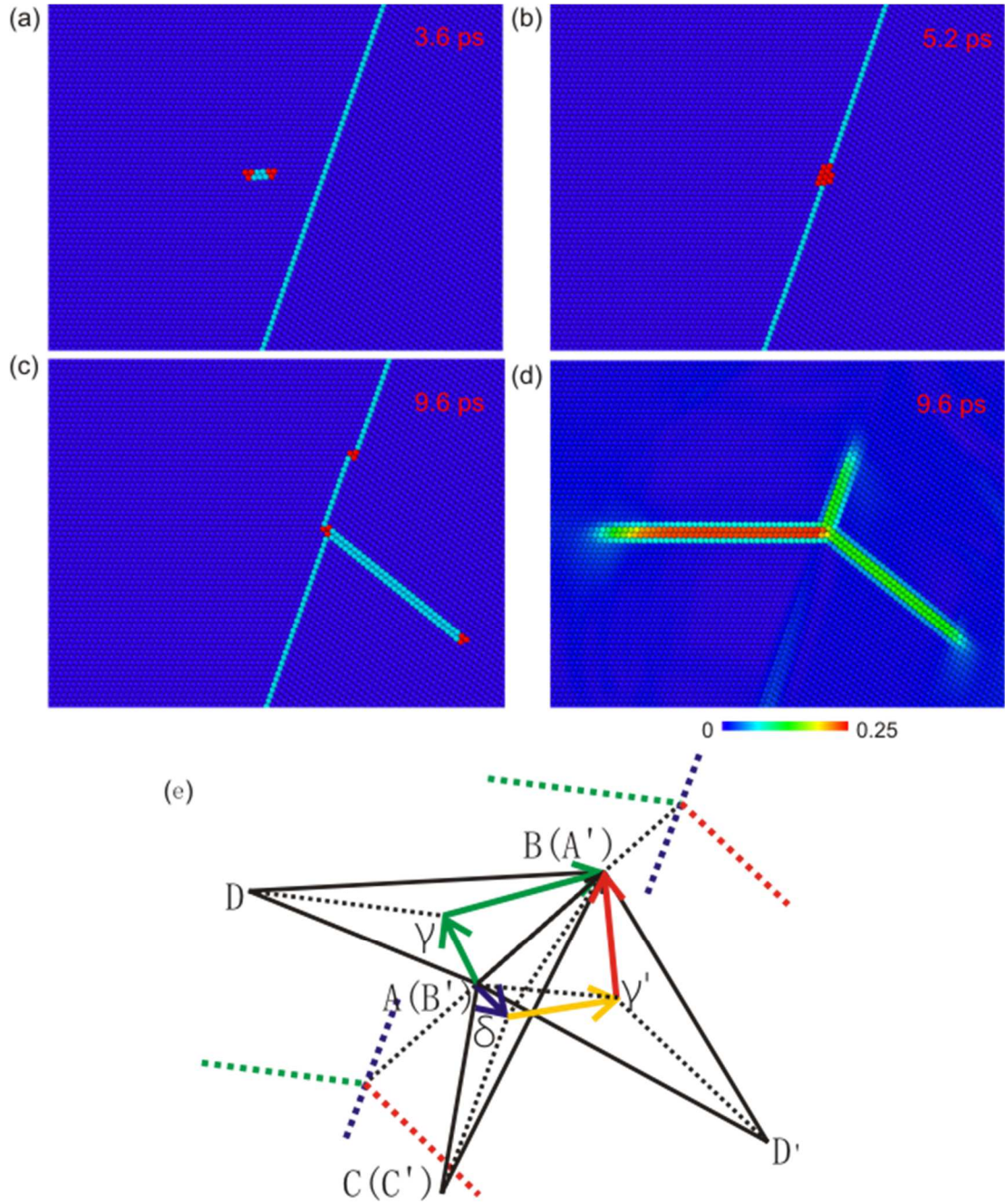


Figure 12. Interaction of screw dislocation with perfect CTB under shear strain of 2.41%. (a) CNA at 3.6 ps; (b) CNA at 5.2 ps, dissociated screw dislocation combine into a full dislocation at CTB; (c) CNA at 9.6 ps, there is one partial dislocation on CTB and another partial dislocation in twin grain connected by a stair-rod dislocation at CTB; (d) Atomic strain at 9.6 ps. This mechanism is referred to as Mechanism L.

3.2. Generalized stacking/twinning fault energy curves

From the three deformation mechanisms above, we can conclude that there are two pathways for newly generated partial dislocations, one is the along the CTB, the other is the slip plane in the twin grain. Under a constant shear strain ε_{yz} , the resolved shear strain on the CTB and the twin grain slip plane is $\frac{1}{3}\varepsilon_{yz}$ and $\frac{7}{9}\varepsilon_{yz}$ respectively. Shear stress can be expressed by $\tau = \mu\varepsilon$, where μ is the shear modulus, and it is the same for this two pathways. Apparently, the resolved shear stress along the slip plane in twin grain would be more than twice as large as the one on CTB. Under shear strain of 0.80%, however, partial dislocations would prefer to dissociate on the CTB regardless of the relative lower shear stress. This could be explained with generalized stacking/twinning fault energy (SFE/TFE) curves as proposed by Jin et al.[9]

Two different models as shown in Figure 13(a) (single crystal) and Figure 13(d) (bicrystal with a CTB in the middle) were implemented to find generalized SFE/TFE curves. The size of the model is 17.71 nm, 16.36 nm and 2.08 nm along x , y , z directions respectively. The lattice orientation in single crystal and the lower part of bicrystal is $x[112]$, $y[\bar{1}10]$, $z[111]$, in the upper part of bicrystal is $x[\bar{1}\bar{1}2]$, $y[1\bar{1}0]$, $z[111]$. To eliminate the side effects, periodic boundary conditions were imposed in x and y directions.

All the atoms in the lower block below the horizontal line in the middle of each model are fixed. Rigid displacement was applied to all the atoms in the upper block above the black horizontal line. The direction of displacement was along the path of minimum energy barrier in the specific lattice structure, i.e. along x direction in single crystal

model, and 60 degree from x to y axis in bicrystal model. A total displacement of $\frac{\sqrt{6}}{6}a_0$ (b_s) was achieved in 50 timesteps (stepsize 0.005 ps), minimization via conjugate gradient method was applied after each timestep.

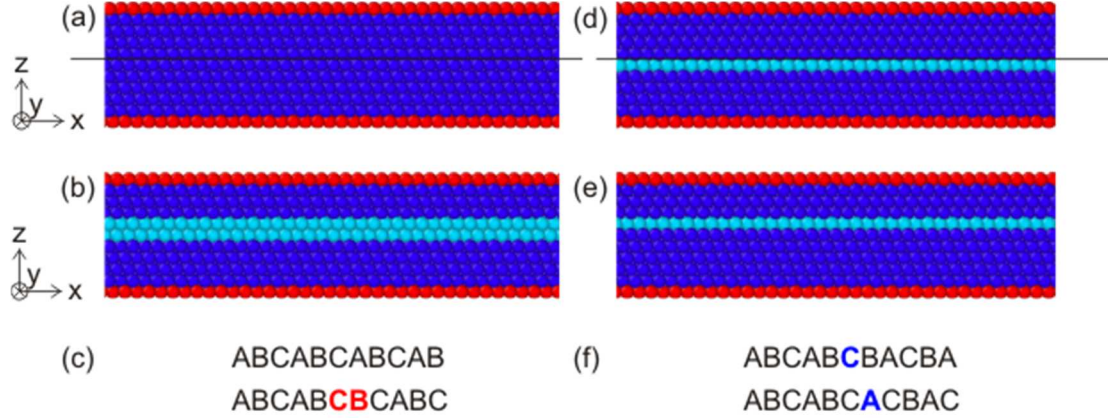


Figure 13. Model for calculating generalized stacking/twinning fault energy curve. (a) Single crystal; (b) After rigid displacement in single crystal, a stacking fault is generated; (c) Staking sequence before (upper) and after (lower) rigid displacement in single crystal; (d) Bi-crystal separated by coherent twin boundary; (e) After rigid displacement, coherent twin boundary moves up by one atomic layer; (f) Staking sequence before (upper) and after (lower) rigid displacement in bi-crystal.

The energy is calculated by summing up the potential energy of all the atoms in the model, the initial energy of the single crystal model is used as a zero level. The total potential energy is then divided by the area in x - y plane. A generalized SFE/TFE curve is generated as shown in Figure 13. In the generalized SFE curve, the peak represents the unstable SFE γ_{US} (162.51 mJm^{-2}), the lowest point after rigid displacement represents the intrinsic SFE γ_S (44.35 mJm^{-2}). In generalized TFE curve, the peak represents the unstable TFE γ_{UT} (139.11 mJm^{-2}). The model after the displacement is shown in Figure 13(b) and 13(e), a staking fault is formed in the single crystal model; twin plane is moved upward by one atomic layer in the bicrystal model.

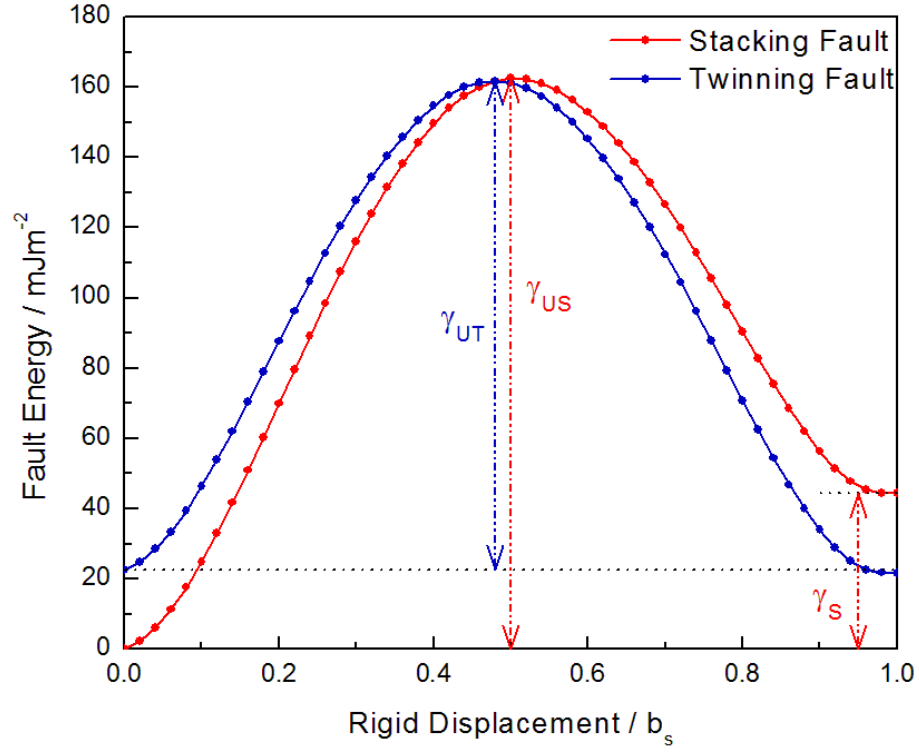


Figure 14. Generalized stacking/twinning fault energy curves.

In Mechanism D, CTB is moved one atomic layer along its normal plane, this is similar to the change in the bicrystal model. Hence, the energy barrier in this reaction can be represented by the generalized twinning fault energy to some degree. In mechanism T, a new stacking fault is formed in the twin grain, this is similar to the change in the single crystal model. Hence, the energy barrier in this reaction can be represented by the generalized stacking fault energy. The dislocation elastic energy released from this two mechanisms is the same ($\frac{a_0^2}{2} > \frac{a_0^2}{6} + \frac{a_0^2}{6}$). A comparison between $\gamma_{US} - \gamma_S = 118.16 \text{ mJm}^{-2}$ and $\gamma_{UT} - \gamma_S = 94.76 \text{ mJm}^{-2}$ (Energy barrier minus the stacking fault energy from the original dissociated screw dislocation) reveals that dissociation on the CTB is energetically favorable. As a result, under lower shear strain, full dislocation

would prefer to dissociate on the CTB. If a larger strain is applied, the dislocation would transmit into the twin grain due to the much larger resolved shear stress.

In Mechanism L, the dislocation elastic energy released ($\frac{a_0^2}{2} > \frac{a_0^2}{6} + \frac{a_0^2}{6} + \frac{a_0^2}{18}$) is lower, while the energy barrier estimation from SFE/TFE ($\gamma_{UT} + \gamma_{US} - \gamma_S = 257.27 \text{ mJm}^{-2}$) is much higher than the other two mechanisms. As a result, a larger strain is needed to activate this mechanism.

In the study by Jin et al.[9], the original Mishin potential, which was fitted using room temperature properties, was modified to refit 0 K properties, the new unstable SFE, unstable TFE and intrinsic SFE were 185.18 mJm^{-2} , 168.68 mJm^{-2} and 29.50 mJm^{-2} respectively. $\gamma_{UT} + \gamma_{US} - \gamma_S$ was 324.36 mJm^{-2} , which was higher than the one above in this present study. Hence, it makes sense that mechanism L was not observed by them. 0 K simulation with unrefitted Mishin potential here can be a theoretical prediction of the mechanisms under ambient temperature without the effect of thermally caused cross slip.

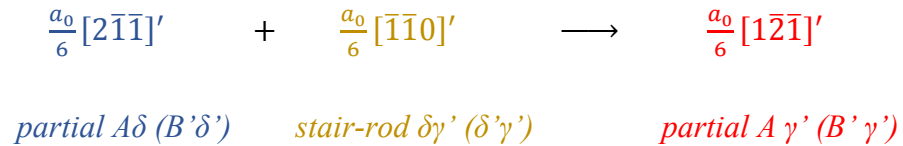
CHAPTER 4: COHERENT TWIN BOUNDARY WITH KINK-LIKE DEFECT

4.1. Influence of kink-like defect on interaction mechanism

4.1.1. 0 degree kink

When a screw dislocation does not come into direct contact with a kink step, i.e. x equal 7.06 nm or 3.08 nm as shown in Figure 8(b) and Figure 8(c), the 0 degree kink does not have a strong influence on the interaction mechanism. Under shear strain of 0.80%, 1.21%, 1.61%, 2.01% and 2.81%, the interaction mechanism is the same as that with perfect CTB.

Under shear strain of 2.41%, nevertheless, when Mechanism L is observed in the perfect CTB model, interaction mechanism evolved from Mechanism L to Mechanism T, as shown in Figure 15(c) and 15(e), the Lomer-lock formed before is unlocked. In Figure 15(d) and 15(f), the atomic strain shown in the yellow box goes from 0.125 at 7.6 ps back to 0 at 11.6 ps. This indicates that the partial on the CTB which first moves upward along the CTB moved back. It combined with the stair-rod, and formed a new trailing partial that is transmitted into the twin grain. This reaction can be expressed as:



Detwinning is observed here due to the migration of kink. It is generally accepted that detwinning, i.e. migration of CTB along its normal direction, either thickening or thinning a twin, is accomplished by the glide of twinning dislocations on the twin

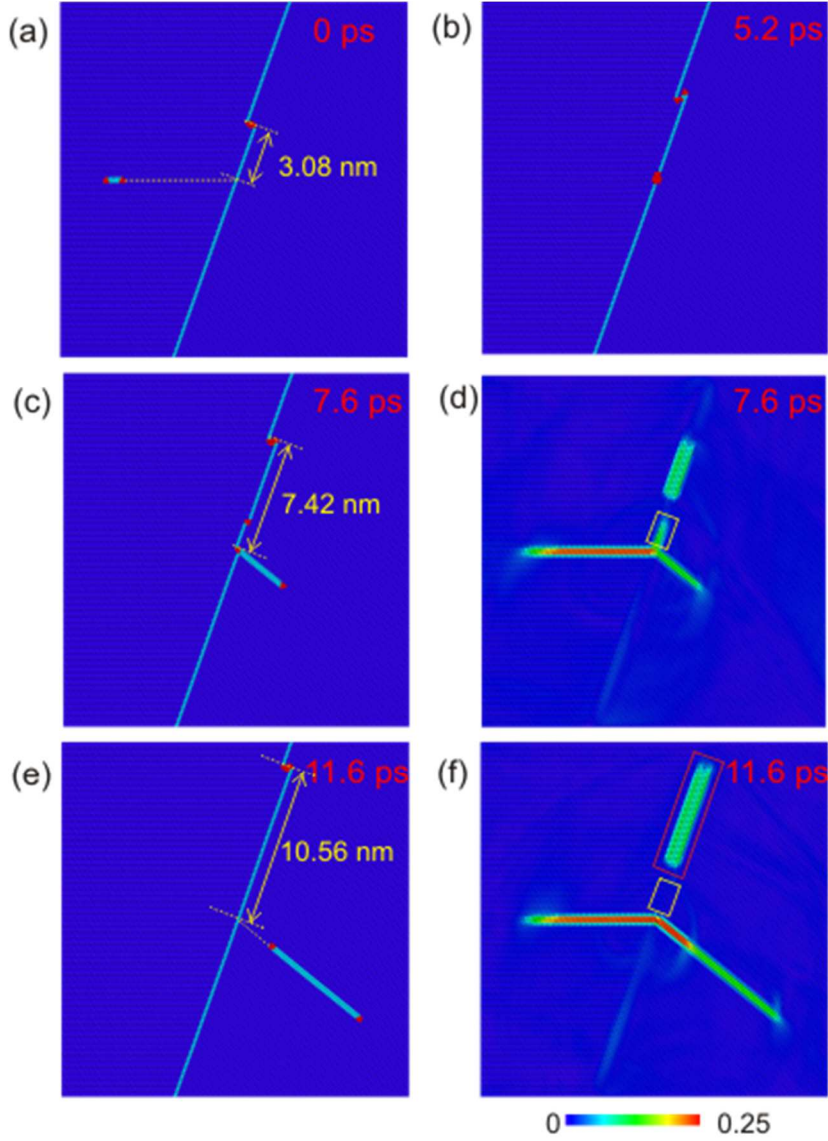


Figure 15. Interaction of screw dislocation with 0 degree kinked ($x=3.08$ nm) CTB under shear strain of 2.41%. (a) CNA at 0 ps; (b) CNA at 4.2 ps, dissociated screw dislocation combine into a full dislocation at CTB; (c) CNA at 7.6 ps, full dislocation becomes one partial on CTB and one partial in twin grain connected by a stair-rod dislocation at CTB; (d) atomic strain at 7.6 ps; (e) CNA at 11.6 ps, the partial dislocation and stair-rod dislocation on CTB re-combine into another partial dislocation which transmits to the twin grain; (f) atomic strain at 11.6 ps.

boundary plane, the twinning dislocations could either nucleate from grain boundary[38–40] or form as a result of reaction of lattice glide dislocations with twin boundaries[9,37,41] like in Mechanism D and Mechanism L. Detwinning caused by twinning dislocation will migrate CTB by only one atomic layer at a time, the migration

of CTB caused by kink here is three atomic layers since there are three dislocations in the kink. This kind of detwinning has been proposed by Lu in studying the thermal stability of ITB.[42]

The migration of kink may explain the reason why the interaction mechanism evolved from L to P. As discussed in Chapter 3, Mechanism L needs more energy than Mechanism T. Since the migration of kink would consume some energy of the system, it is more difficult for Mechanism L to occur.

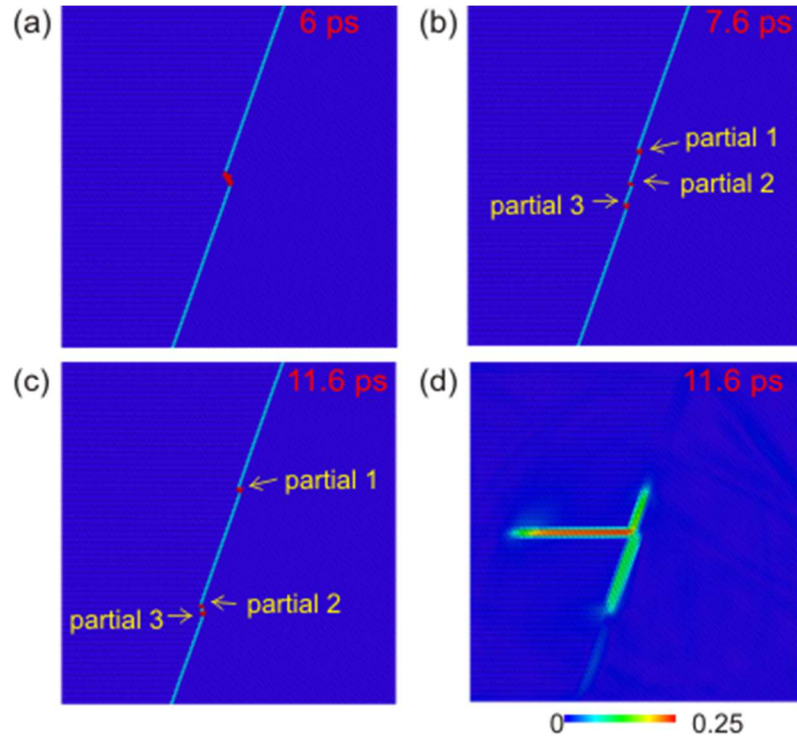


Figure 16. Interaction of screw dislocation with 0 degree kinked ($x=0$ nm) coherent twin boundary under shear strain of 0.80%. (a) CNA at 5.6 ps, screw dislocation recombines at twin boundary; (b) CNA at 7.6 ps, three partial dislocations are generated on twin boundary; (c) CNA at 11.6 ps, partial dislocation 1 moves in one direction, while partial dislocation 2 and 3 move in another direction; (d) Atomic strain at 11.6 ps. This mechanism is referred to as Mechanism D'.

When screw dislocation come into direct contact with the kink, i.e. x equals 0 nm, the kink would have a strong influence on the deformation mechanism.

Figure 16 shows the interaction under shear strain of 0.80%. While Mechanism D is observed in the case of perfect CTB, a new dissociation mechanism is found here. At 6 ps, full dislocation combine with the kink and becomes a new ‘kink’. Then this new ‘kink’ would dissociate into three partial dislocations (partial 1, partial 2, partial 3) as shown in Figure 16(b-c), partial 1 would move upwards along the twin boundary, while partial 2 and partial 3 would move downwards along the twin boundary. In this new mechanism, a staircase-like structure is formed by detwinning with the partials forming the steps. This mechanism is referred to as Mechanism D’ in the following context. The same mechanism is observed under shear strain of 1.21% and 1.61%, while Mechanism T is observed in the case of perfect CTB.

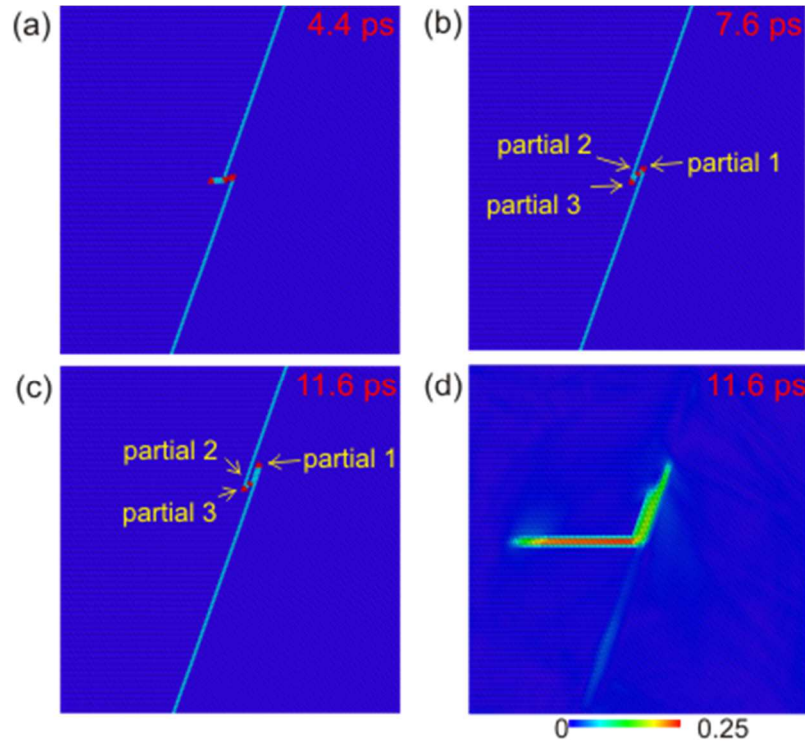


Figure 17. Interaction of screw dislocation with 0 degree kinked ($x=0$ nm) coherent twin boundary under shear strain of 2.41%. (a) CNA at 4.4 ps; (b) CNA at 7.6 ps, three partial dislocations are generated on twin boundary; (c) CNA at 11.6 ps, three partial dislocations moves in the same direction; (d) atomic strain at 11.6 ps. This mechanism is referred to as Mechanism D’.

Under shear strain of 2.01% and 2.41%, when Mechanism T and Mechanism L was observed in the case of CTB, another new dissociation mechanism was found as shown in Figure 17. After the screw dislocation recombines near the kink, the new ‘kink’ becomes three partial dislocations that moves in the same direction. This is referred to as Mechanism D’’ in the following context.

Figure 18 is the Thompson tetrahedron illustration of these two new interaction mechanisms. As discussed in 2.2.4, the kink is composed of three partial dislocations whose Burgers vector adds up to zero. Hence, the dislocations before reaction can be represented by Figure 18(a) where 5 partial dislocations exist. After reaction, only 3 dislocations are observed on the twin plane. Two possible configuration of the Burger’s vector of them are shown in Figure 18(b) and 18(c). Which one represents Mechanism D’ or Mechanism D’’ should be determined by the forces on the dislocations, and is not discussed here. The reaction equation shows the elastic energy of dislocation decreases in these two mechanisms ($5 * \frac{a_0^2}{6} > 3 * \frac{a_0^2}{6}$). As a comparison, there is no change in Mechanism D and T, and would even increase ($2 * \frac{a_0^2}{6} < 2 * \frac{a_0^2}{6} + \frac{a_0^2}{18}$) in Mechanism T, this may explain why Mechanism D’ and D’’ are favored until a shear strain up to 2.41% in 0 degree kinked CTB when $x=0$ nm.

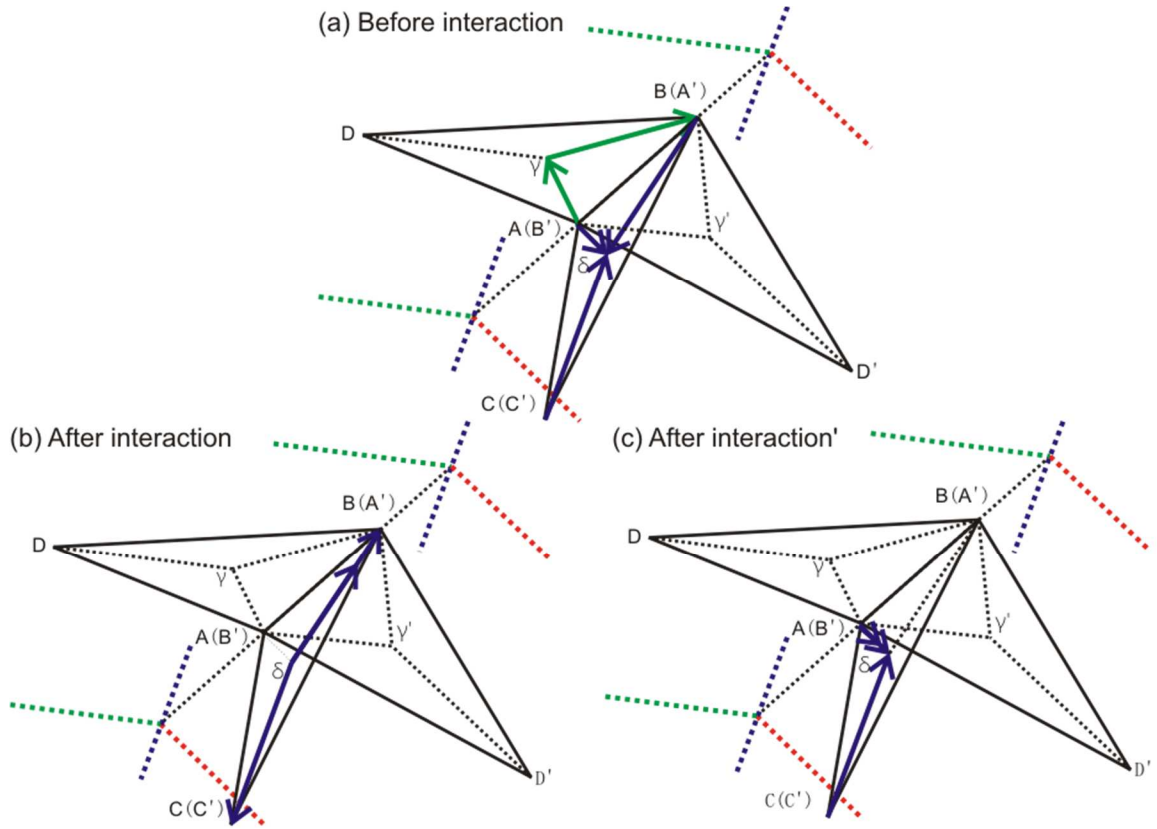


Figure 18. Thompson tetrahedron illustration of interaction mechanisms between screw dislocation and 0 degree kinked CTB. Burgers vectors of partial dislocations (a) before interaction; (b-c) after interaction.

$$\frac{a_0}{6} [\bar{2}1\bar{1}] + \frac{a_0}{6} [\bar{1}21] + \frac{a_0}{6} [\bar{1}21] + \frac{a_0}{6} [2\bar{1}\bar{1}] + \frac{a_0}{6} [\bar{1}\bar{1}2]$$

$$\text{Partial } Ay + \text{Partial } \gamma B + \text{Partial } A\delta + \text{Partial } B\delta + \text{Partial } C\delta$$

$$\longrightarrow \frac{a_0}{6} [11\bar{2}] + \frac{a_0}{6} [\bar{2}11] + \frac{a_0}{6} [\bar{2}11]$$

$$\text{Partial } \delta C + \text{Partial } \delta B + \text{Partial } \delta B$$

$$\longrightarrow \frac{a_0}{6} [\bar{1}\bar{1}2] + \frac{a_0}{6} [\bar{1}2\bar{1}] + \frac{a_0}{6} [\bar{1}2\bar{1}]$$

$$\text{Partial } C\delta + \text{Partial } A\delta + \text{Partial } A\delta$$

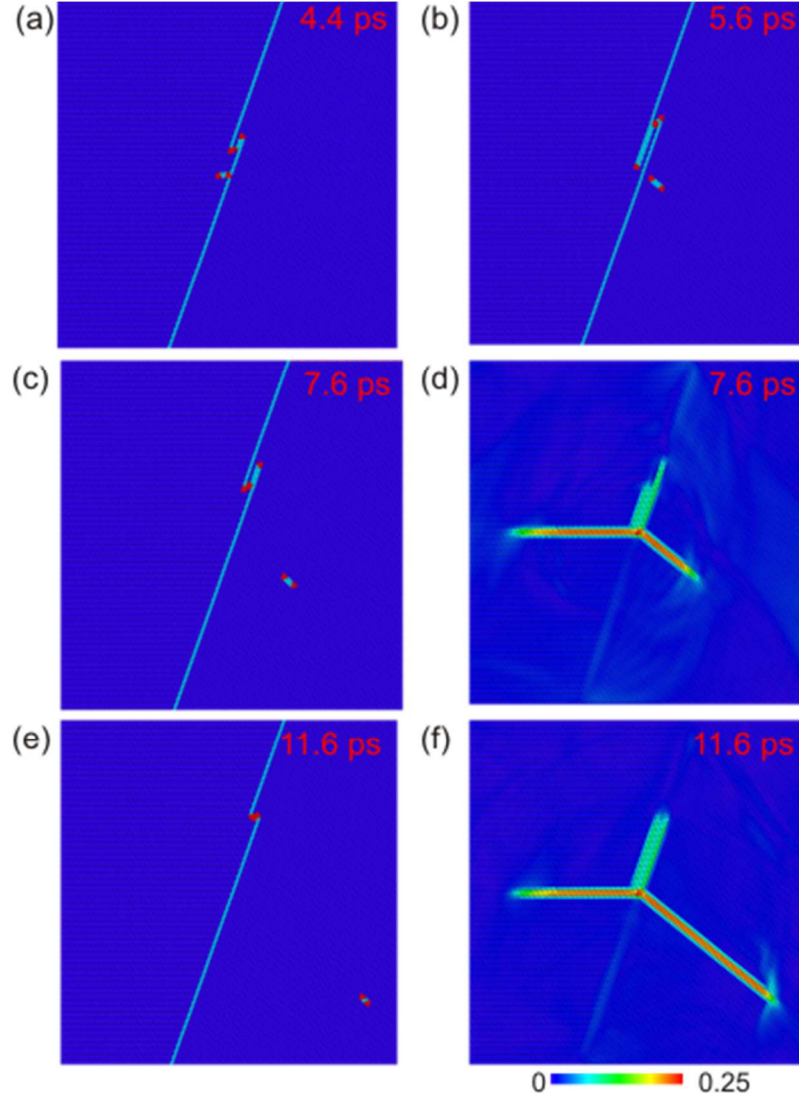


Figure 19. Interaction of screw dislocation with 0 degree kinked ($x=0$ nm) CTB under shear strain of 3.62%. (a) CNA at 4.4 ps, kink moves upwards under shear strain, steps are formed in kink ; (b) CNA at 5.6 ps, screw dislocation transmits into the twin grain; (c) CNA at 7.6 ps; (d) Atomic strain at 7.6 ps; (e) CNA at 11.6 ps, steps on kink disappear; (f) Atomic strain at 11.6 ps.

Under shear strain of 2.81% or even higher strain of 4.80%, when Mechanism L takes place in the case of CTB, screw dislocation would interact with twin boundary by Mechanism T. Figure 19 is the snapshots of interaction under shear strain of 3.62%. Under such high shear strain, Mechanism D' and Mechanism D'' cannot occur, because as kink migrates, dislocation cannot interact directly with kink.

It is worth noting that the partial dislocations in the kink does not migrate concurrently. At 4.4 ps, one partial is emitted from the kink; at 5.6 ps, the partial in the middle catches up; at 7.6 ps, the third partial catches up; they get together again at 11.6 ps. This is also observed in Figure 15 actually, however, it is more obvious here since the shear strain is higher. This phenomena could explained by the force on dislocations. According to elastic theory, these three dislocations are attractive to each other since they each have an opposite Burgers vector component, they have a tendency to stay together. Dislocations here, however, are subject to applied shear stress, interface tension of the stacking fault formed when the partial dislocation glides away from the kink, the Peierls force or other friction type force[43,44] aside from dislocation interaction force. A detailed analysis of the effect of these stresses on kink migration is out of the scope of this thesis.

4.1.2. 60 degree kink

When a dislocation interact with a 60 degree kinked CTB, there is always direct intersection with the kink. The screw dislocation is divided in to three segments by the two kinks in this model as shown in Figure 20(a): one in the middle, the other two on the left and right (the left and right can be regarded as one segment because the model is periodic in y direction). Figure 8(f) shows the viewing angle for the snapshots in the following figures. Snapshots in the left column are taken from View 1, snapshots are the right column is taken from View 2. DXA was applied to some of the models, green, red, blue line represents Shockley partials, full dislocation, stair-rod dislocation respectively.

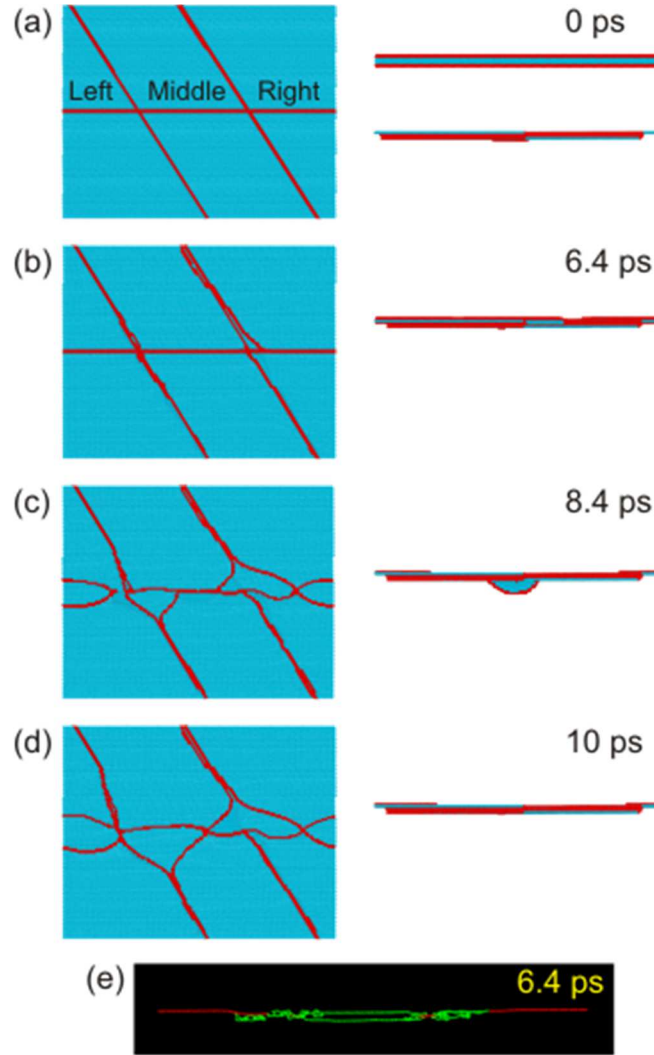


Figure 20. Interaction of screw dislocation with 60 degree kinked coherent twin boundary under shear strain of 0.80%. (a) CNA at 0 ps; (b) CNA at 6.4 ps; (c) CNA at 8.4 ps; (d) CNA at 10 ps; (e) DXA at 6.4 ps.

Under shear strain of 0.80%, all the segments of screw dislocation would dissociate on the twin plane by Mechanism D. At 6.4 ps, left and right segments of screw dislocation recombines to full dislocation at twin boundary, while the middle segment is still two partials as shown by DXA in Figure 20(e). This is because left and right segments of screw dislocation would come into contact with the twin boundary sooner because of the four atomic layer high step due to the kink. At 8.4 ps, there is a little bit

of transmission in the middle segment, but it disappears quickly. The dislocations keeps migrating on the twin plane in the following simulation time.

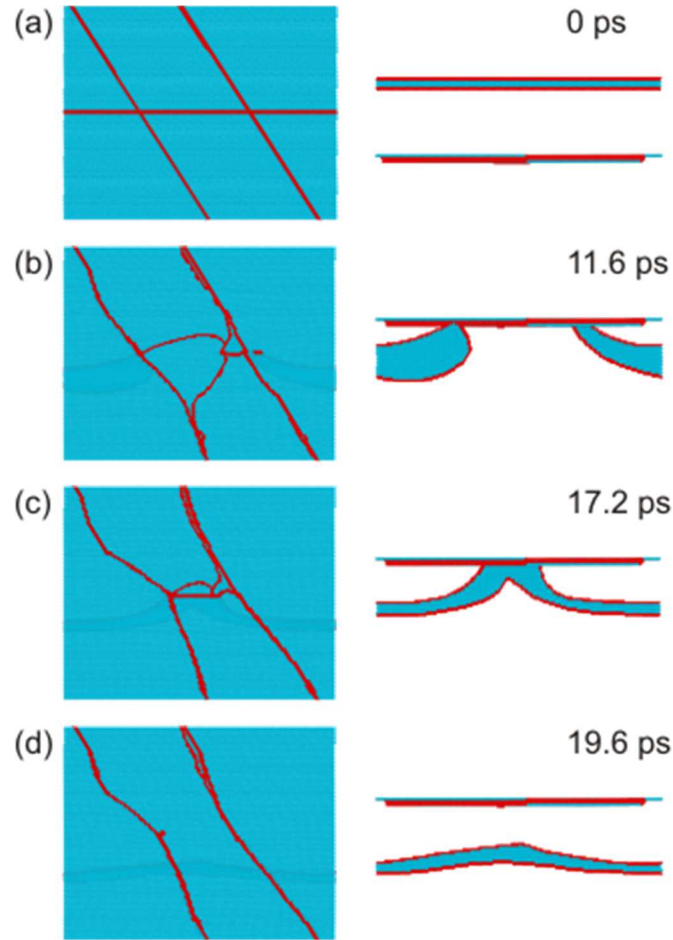


Figure 21. Interaction of screw dislocation with 60 degree kinked coherent twin boundary under shear strain of 1.21%. (a) CNA at 0 ps; (b) CNA at 11.6 ps; (c) CNA at 17.2 ps; (d) CNA at 19.6 ps.

Under shear strain of 1.21%, the middle segment of dislocation would dissociate on the twin boundary by Mechanism D, while the left and right segments would transmit to the twin grain by Mechanism T, and the ends of the transmitted dislocations are pinned near the kink as shown in Figure 21(b). As relaxation continues, the pinning point of penetrated dislocations start moving towards the middle as shown in Figure 21(c). Finally the partials in the middle segment disappear, partitioned dislocations become one full

dislocation in twin grain in Figure 21(d), and the kinked twin boundary almost goes back to its original structure. The same mechanism takes place under shear strain of 1.61%.

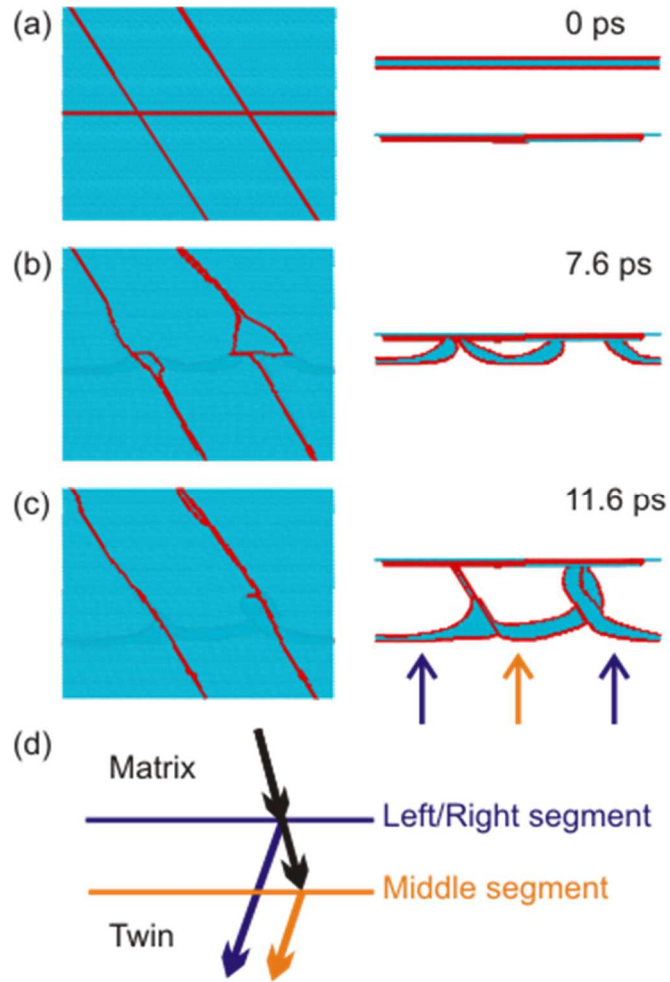


Figure 22. Interaction of screw dislocation with 60 degree kinked coherent twin boundary under shear strain of 2.01%. (a) CNA at 0 ps; (b) CNA at 7.6 ps; (c) CNA at 11.6 ps; (d) A schematic illustration of screw dislocation intersecting with twin boundary on different plane.

Under shear strain of 2.01%, Mechanism T is observed in all the segments. The newly formed dissociated partials in the twin grain are actually on different planes as illustrated schematically in Figure 22(d). The middle segment would interact with a twin boundary that is four atom layers lower than that of left/right segment, hence, the

transmitted dislocation would be on different plane. Another thing to note here is that the dislocations never gets unpinned from the kink like the case in Figure 22.

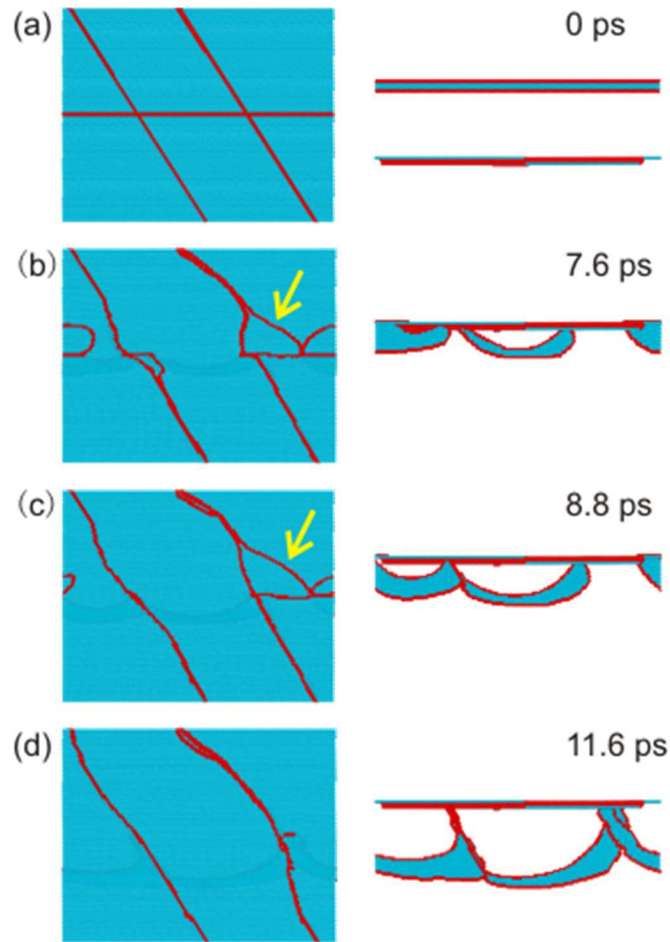


Figure 23. Interaction of screw dislocation with 60 degree kinked coherent twin boundary under shear strain of 2.41%. (a) CNA at 0 ps; (b) CNA at 7.6 ps; (c) CNA at 8.8 ps; (d) CNA at 11.6 ps. Yellow arrow indicates the partial emitted from kink.

Under shear strain of 2.41%, the middle segment would transmit to the twin grain, while the left and right would react by Mechanism L. However, the Lomer-lock is not stable here, it will be unlocked latter and become the transmission structure with pinning at the kink similar to the case in Figure 22 as shown in Figure 23(d). Partial dislocations

emitted from the kink as indicated by the yellow arrow in Figure 22(b-c) should play an important role in this unlocking process.

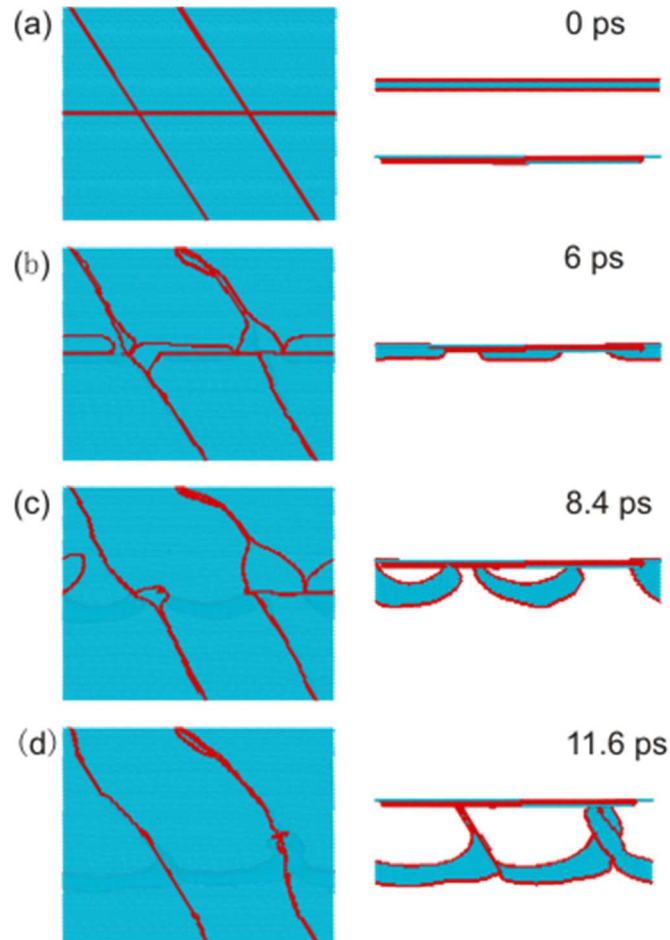


Figure 24. Interaction of screw dislocation with 60 degree kinked coherent twin boundary under shear strain of 2.81%. (a) CNA at 0 ps; (b) CNA at 6 ps; (c) CNA at 8.4 ps; (d) CNA at 11.6 ps.

Under shear strain of 2.81%, all the dislocation segments react by the Mechanism L. As the relaxation continues, all the Lomer-locks gradually disappear, and finally becomes a structure similar to the one observed under shear strain of 2.01% too. A DXA for this case is shown in Figure 25.

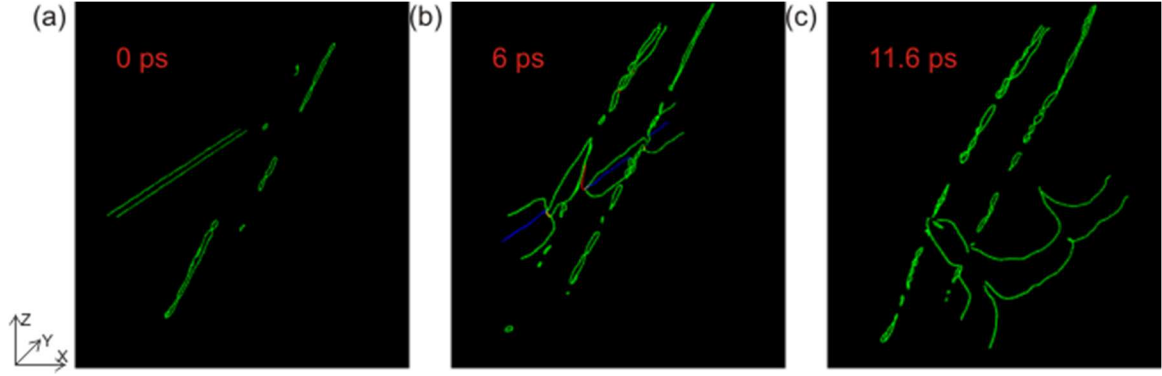


Figure 25. DXA of interaction of screw dislocation with 60 degree kinked coherent twin boundary under shear strain of 2.81%.

As discussed in Chapter 3, interaction goes from Mechanism D, Mechanism T to Mechanism L as strain increases. The results in the case of 60 degree kinked CTB are in accordance with this conclusion. It is worth mentioning that the mechanism in the middle segment might be different than that in the left/right segment, as in the case of 1.21% and 2.41% shear strain. This make sense because the left/right segment interact with the twin boundary sooner.

4.1.3. Summary

Table 1 is a summarization of all the interaction mechanisms under various shear strain for perfect CTB, 0 degree kinked CTB at different locations and 60 degree kinked CTB.

Table 1. Interaction mechanism between screw dislocation and perfect/0 degree kinked/60 degree kinked coherent twin boundaries under various shear strains.

Shear Strain	Perfect CTB	0° Kinked CTB $x=7.06$ nm	0° Kinked CTB $x=3.08$ nm	0° Kinked CTB $x=0$ nm	60° Kinked CTB
0.80%	D	D	D	D'	D
1.21%	T	T	T	D'	First D/T, then T (no pinning)
1.61%	T	T	T	D'	First D/T, then T (no pinning)
2.01%	T	T	T	D''	T (pinning)
2.41%	L	First L, then T	First L, then T	D''	First T/L, then T (pinning)
2.81%	L	L	L	T	First L, then T (pinning)

4.2. Influence of kink-like defect on the mechanical behavior

This section discusses the effect of the kink-like defect on the mechanical behavior via a comparison of the variation of von-Mises stress over time under different shear strain including all the models studied (Perfect CTB, 0° kinked CTB with $x = 7.06$ nm, 0° kinked CTB with $x = 3.08$ nm, 0° kinked CTB with $x = 0$ nm, 60° kinked CTB). Under the same applied shear strain, a larger von-Mises stress would suggest a stronger strengthening effect.

In order to have a clearer view of the differences between these 5 models after interaction, the curve before 4 ps are not shown since they are almost the same for all models. A grey background is added to the area after interaction, Linear fit are applied to all the curves after 7.6 ps, and the slope of the linear fit lines are listed Table 2-6.

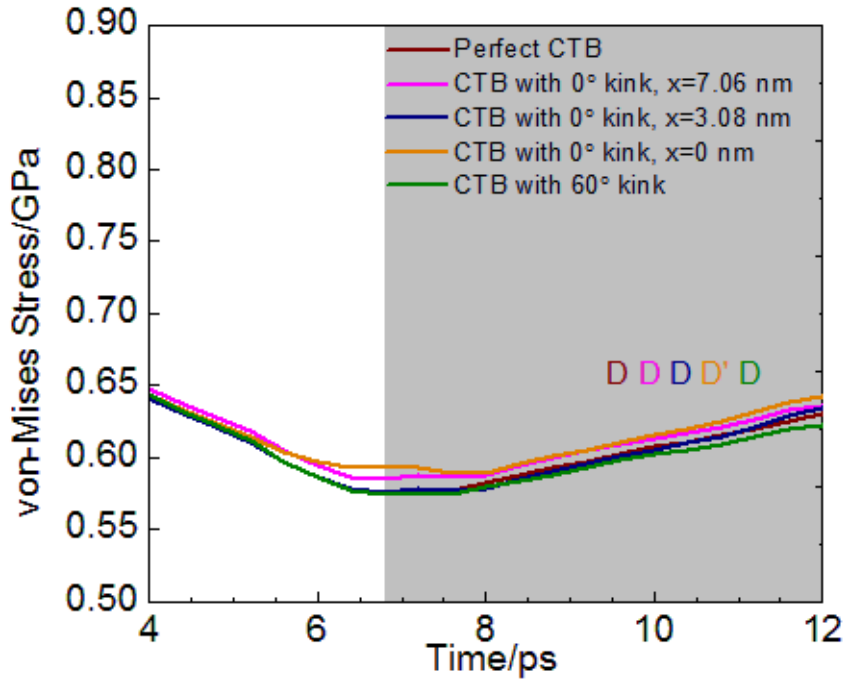


Figure 26. Variation of von-Mises stress over time under shear strain of 0.80%.

Table 2. Linear fit trend line slope after 7.6 ps in different models and a comparison with the case of perfect CTB under shear strain of 0.80%.

Shear 0.80%	Perfect CTB	0 kink $x=7.06$ nm	0 kink $x=3.08$ nm	0 kink $x=0$ nm	60 kink
Slope	0.01191	0.01149	0.01326	0.01261	0.01085
Increase	-	-3.53%	11.33%	5.87%	8.90%

Under shear strain of 0.80%, dislocation would dissociate into the twin boundary in all the models. Although the mechanism is different in the model of 0° kinked CTB with $x=0$ nm (Mechanism D') compared to other models (Mechanism D), the stress-time curve of all these cases are similar as shown in Figure 26. This indicates that the Mechanism D and Mechanism D' has the same strengthening effect, and presence of kink defects has no significant impact on mechanical behavior under this loading condition.

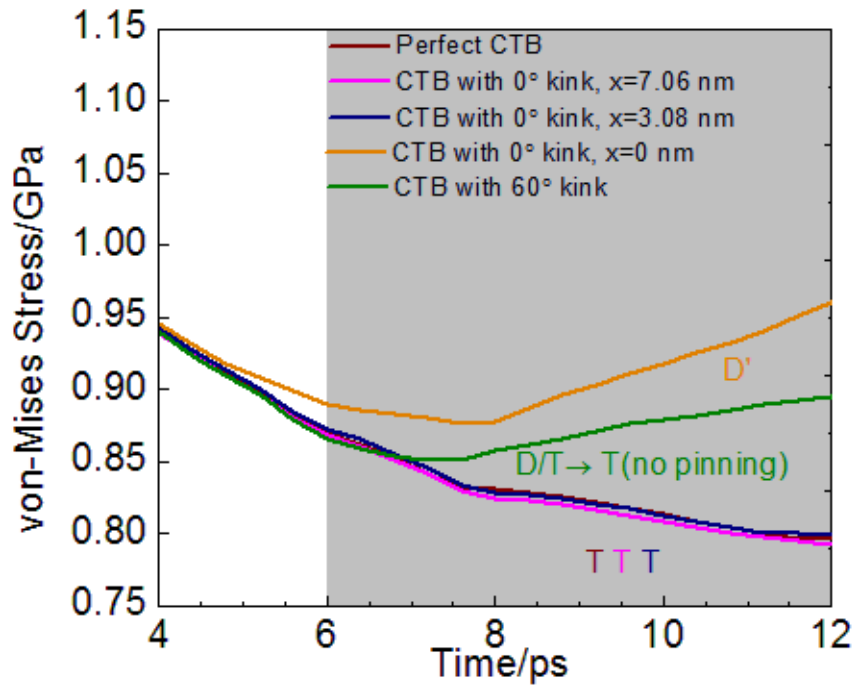


Figure 27. Variation of von-Mises stress over time under shear strain of 1.21%.

Table 3. Linear fit trend line slope after 7.6 ps in different models and a comparison with the case of perfect CTB under shear strain of 1.21%.

Shear 1.21%	Perfect CTB	0 kink $x=7.06$ nm	0 kink $x=3.08$ nm	0 kink $x=0$ nm	60 kink
Slope	-0.00901	-0.00873	-0.00829	0.01954	0.00985
Increase	-	3.12%	7.99%	316.87%	209.32%

Under shear strain of 1.21%, Mechanism T is observed in Perfect CTB, 0° kinked CTB with $x=7.06$ nm and 0° kinked CTB with $x=3.08$ nm, and the slopes of them are close. The slope of 0° kinked CTB with $x=0$ nm and 60° kinked CTB is more than 3 times and 2 times higher than the case of perfect CTB, respectively. Mechanism D' occurs in the model of 0° kinked CTB with $x=0$ nm, and this model has the largest strengthening effect. The 60° kinked CTB model is the medium one because it evolved from Mechanism D/T to T. This case provides evidence that Mechanism D/D' has more hardening effect than T. Similar results are obtained under shear strain of 1.61%.

Under shear strain of 2.01%, dislocation would dissociate on the twin boundary in the case of 0° kinked CTB with $x=0$ by Mechanism D'', Mechanism T takes place in all other cases. The slope of linear fit line in the case of 0° kinked CTB with $x=0$ nm increased by 692.96% compared with perfect CTB, which is much higher than all the other as listed in Table 4. Apparently, Mechanism D'' has a much more significant hardening effect than Mechanism T. In the case of 60° kinked CTB, transmitted dislocation is divided into three segments with two pinning points at the kink as shown

in Figure 22. Hence, it make sense that the 60° kinked stress-time curve (green) is slightly higher than the others with Mechanism T due to the hardening caused by the pinning.

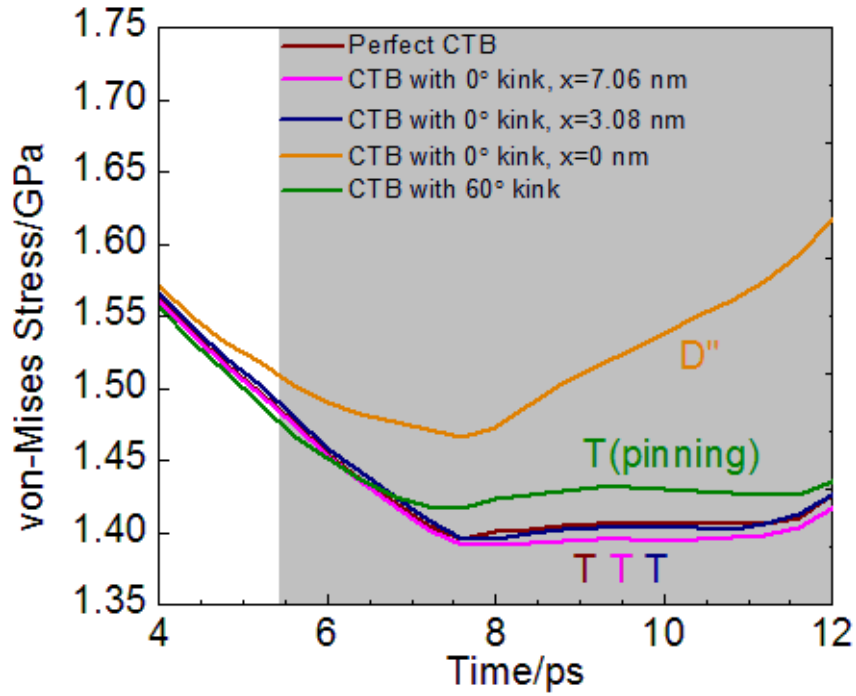


Figure 28. Variation of von-Mises stress over time under shear strain of 2.01%.

Table 4. Linear fit trend line slope after 7.6 ps in different models and a comparison with the case of perfect CTB under shear strain of 2.01%.

Shear 2.01%	Perfect CTB	0 kink $x=7.06$ nm	0 kink $x=3.08$ nm	0 kink $x=0$ nm	60 kink
Slope	0.00412	0.00380	0.00480	0.03267	0.00184
Increase	-	-7.77%	16.50%	692.96%	-55.34%

Under shear strain of 2.41%, Mechanism D'' still occurs in the case of 0° kinked CTB with $x=0$. In perfect CTB, Mechanism L is observed. In all other cases, total or part of the dislocation goes under Mechanism L first, but finally evolved to Mechanism T.

From Figure 29 and Table 5, it is apparent that, Mechanism L has larger strengthening effect than Mechanism T, while D'' has the highest strengthening effect.

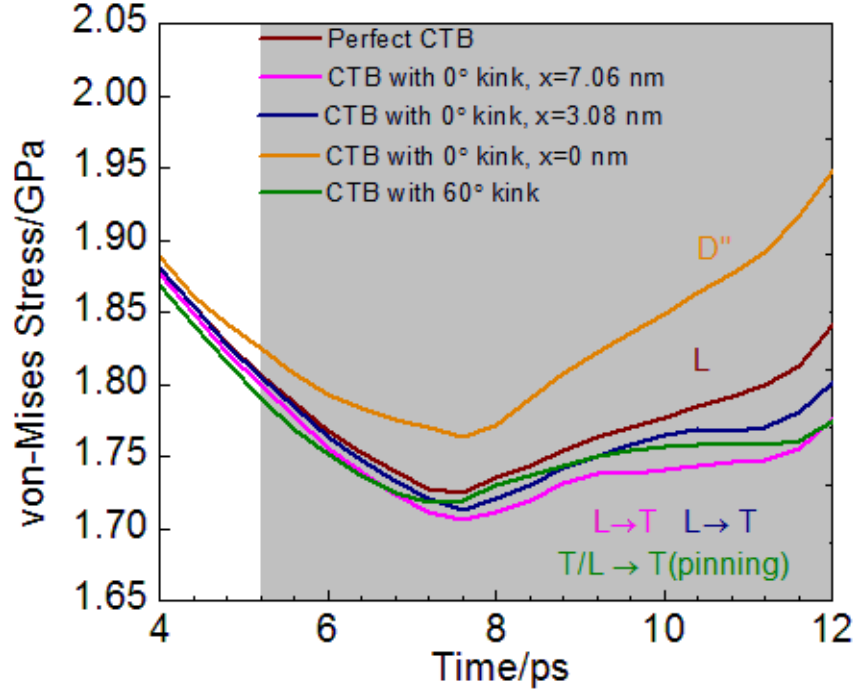


Figure 29. Variation of von-Mises stress over time under shear strain of 2.41%.

Table 5. Linear fit trend line slope after 7.6 ps in different models and a comparison with the case without CTB under shear strain of 2.41%.

Shear 2.41%	Perfect CTB	0 kink $x=7.06\text{nm}$	0 kink $x=3.08\text{nm}$	0 kink $x=0\text{nm}$	60 kink
Slope	0.02348	0.01273	0.01741	0.03962	0.00991
Increase	-	-45.78%	-25.85%	68.74%	-57.79%

Under shear strain of 2.81%, Mechanism T is observed in 0° kinked CTB with $x=0$ nm. In all other cases Mechanism L take place, and only the Lomer-lock in 60° kinked CTB is later unlocked. This case could further prove that Mechanism L has larger strengthening effect than Mechanism T. One thing to note here is that although the

increase in slope is lower in 60° kinked CTB than 0° kinked CTB with $x=0$ nm, the stress is higher in the 60° kinked CTB, it has more strengthening effect.

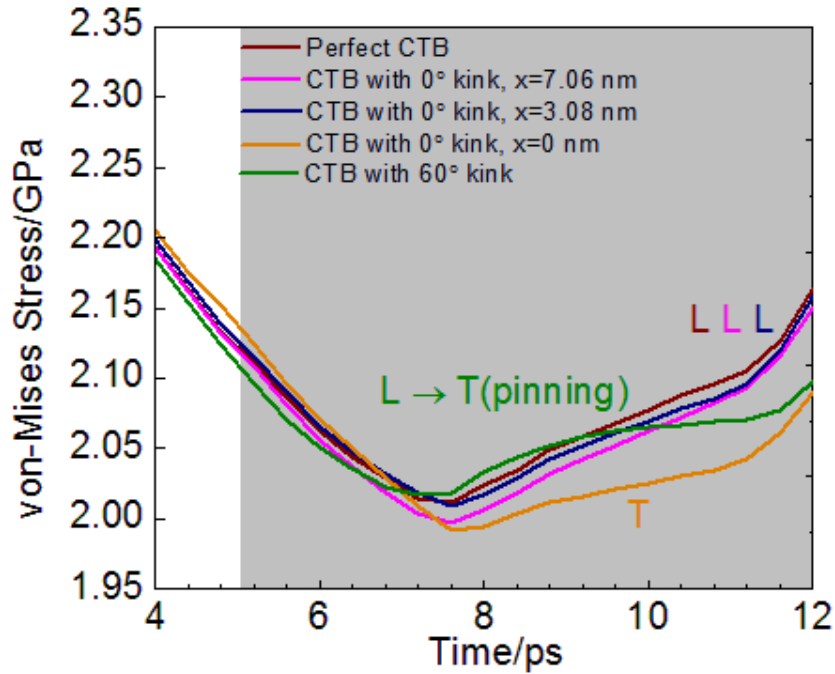


Figure 30. Variation of von-Mises stress over time under shear strain of 2.81%.

Table 6. Linear fit trend line slope after 7.6 ps in different models and a comparison with the case of perfect CTB under shear strain of 2.81%.

Shear 2.41%	Perfect CTB	0 kink $x=7.06\text{nm}$	0 kink $x=3.08\text{nm}$	0 kink $x=0\text{nm}$	60 kink
Slope	0.02993	0.03086	0.02903	0.01847	0.01368
Increase	-	3.11%	-3.01%	-38.29%	-54.29%

To summarize, the strengthening effect in increasing order is found to be:

Mechanism T < Mechanism D/D' and

Mechanism T < Mechanism L < Mechanism D''

Whether the kink would strengthen or soften the material depend on the loading condition.

CHAPTER 5: CONCLUSIONS

Intrinsic kink-like twin boundary defect was recently found in nanotwinned copper.[19] Their influence on the interaction between screw dislocation (Burgers vector parallel to the dislocation line) and CTB was studied by equilibrium MD simulation using simple bicrystal models in copper. It was found that kink-like defects have a profound impact on screw dislocation - CTB interaction mechanism, giving rise to significant strengthening or softening effects.

Mechanism D, Mechanism T and Mechanism L were found to be the three possible interaction mechanisms between a screw dislocation and a perfect CTB. In Mechanism D, recombined full dislocation at CTB dissociate into two partial dislocations that move in opposite directions along the CTB; In mechanism T, recombined full dislocation at CTB transmit and form two partials on the slip plane in twin grain. In Mechanism L, a Lomer-lock is formed by one stair-rod dislocation on the CTB, one partial on the CTB and another partial in twin grain. A rough estimate of energy barrier for these three mechanisms are 94.76 mJm^{-2} , 118.16 mJm^{-2} and 257.27 mJm^{-2} respectively from generalized stacking/twinning fault energy curves, thus an increasing shear strain is needed to activate the Mechanism from D, T to L.

A screw dislocation could be either 0 degree or 60 degree to the kink in the twin boundary. For the 0 degree case, when screw dislocation does not come into direct contact with the kink, a kink defect has little influence on the interaction mechanism. However, as the migration of kink which causes detwinning in the model would consume energy from the system, Mechanism L is found to evolve back to Mechanism T under

shear strain of 2.41%. When screw dislocation come into direct contact with the kink, two new mechanisms, Mechanism D' and Mechanism D'', are introduced. In these two mechanisms, five partial dislocations before interaction become three dislocations. The decrease of dislocation elastic energy in these two cases is relatively higher than that of Mechanism D, T and L. As a result, these two mechanisms are favored until a shear strain up to 2.41%. Under shear strain of 2.81% or higher, Mechanism T is observed. Mechanism L does not occur probably also due to the energy consumed by kink migration.

For the 60 degree case, a screw dislocation is divided into three segments by the two kink steps present in the model. The interaction mechanism varies from D, T to L (which then evolves to T again) as the strain increases. The mechanism in the middle segment is not always the same as that in the left/right segment, because the left/right segment would interact with the twin boundary sooner.

A concise summary on the effect of different types of kink defects on interaction mechanisms can be in Table 1.

From the analysis of von-Mises stress – time curves, it is concluded that the strengthening effect of mechanisms with an increasing order is:

Mechanism T < Mechanism D/D' and

Mechanism T < Mechanism L < Mechanism D''

Whether the kink would strengthen or soften the material depend on the loading condition. Under shear strain of 0.81%, kinks are predicted not to affect the mechanical behavior. Under shear strain of 1.21%, 0° kinked CTB with $x=0$ nm and 60° kinked CTB

are found to significantly strengthen the material. Under shear strain of 2.01%, only 0° kinked CTB with $x=0$ nm could strengthen the material. Under shear strain of 2.41%, a 0° kinked CTB with $x=0$ nm promotes hardening effects, while all the others kink configurations result in softening. Under shear strain of 2.81%, 0° kinked CTB with $x=0$ nm and 60° kinked CTB are found to soften the material.

This study has proved that kink-like defects in CTBs play a significant role in the mechanical behavior of nanotwinned system. CTBs must be considered as defective entities in order to fully understand CTB-strengthened material.

References

- [1] A.H.Cottrell. Dislocations and Plastic Flow in Crystals. 1953.
- [2] Gleiter H. Prog Mater Sci 1990;33:223.
- [3] Lu L, Chen X, Huang X, Lu K. 2009;323:2007.
- [4] Lu L, Shen Y, Chen X, Qian L, Lu K. Science (80-) 2004.
- [5] Sansoz F, Huang H, Warner DH. JOM 2008;60:79.
- [6] Yu Q, Qi L, Chen K, Mishra RK, Li J, Minor AM. Nano Lett 2012;12:887.
- [7] Zhao Y, Furnish TA, Kassner ME, Hodge AM. J Mater Res 2012;27:3049.
- [8] Aubry S, Kimmer C, Skye A, Schelling P. Phys Rev B 2008;78:064112.
- [9] Jin Z-H, Gumbsch P, Ma E, Albe K, Lu K, Hahn H, Gleiter H. Scr Mater 2006;54:1163.
- [10] Jin Z-H, Gumbsch P, Albe K, Ma E, Lu K, Gleiter H, Hahn H. Acta Mater 2008;56:1126.
- [11] Cao a. J, Wei YG, Mao SX. Appl Phys Lett 2007;90:88.
- [12] Deng C, Sansoz F. ACS Nano 2009;3:3001.
- [13] Wu ZX, Zhang YW, Srolovitz DJ. Acta Mater 2009;57:4508.
- [14] Li X, Wei Y, Lu L, Lu K, Gao H. Nature 2010;464:877.
- [15] Chassagne M, Legros M, Rodney D. Acta Mater 2011;59:1456.
- [16] Chen Z, Jin Z, Gao H. Phys Rev B 2007;75:212104.
- [17] Zhu T, Li J, Samanta A, Kim HG, Suresh S. Proc Natl Acad Sci U S A 2007;104:3031.
- [18] Zhu YT, Wu XL, Liao XZ, Narayan J, Kecskés LJ, Mathaudhu SN. Acta Mater 2011;59:812.

- [19] Wang YM, Sansoz F, LaGrange T, Ott RT, Marian J, Barbee TW, Hamza A V. Nat Mater 2013;12:697.
- [20] Alder BJ, Wainwright TE. J Chem Phys 1959;31:459.
- [21] Alder BJ, Wainwright TE. J Chem Phys 1960;33:1439.
- [22] Plimpton SJ. J Comput Phys 1995.
- [23] Mishin Y, Mehl M, Papaconstantopoulos D, Voter a., Kress J. Phys Rev B 2001;63:224106.
- [24] Honeycutt JD, Andemen HC. J Phys Chem 1987;91:4950.
- [25] Faken D, Jónsson H. Comput Mater Sci 1994;2:279.
- [26] Tsuzuki H, Branicio PS, Rino JP. Comput Phys Commun 2007;177:518.
- [27] Stukowski A. Model Simul Mater Sci Eng 2009;18:015012.
- [28] Stukowski A, Albe K. Model Simul Mater Sci Eng 2010;18:085001.
- [29] Stukowski A, Bulatov V V, Arsenlis A. Model Simul Mater Sci Eng 2012.
- [30] Falk ML, Langer JS. 1997;57:16.
- [31] Shimizu F, Ogata S, Li J. Mater Trans 2007;48:2923.
- [32] R.Clausius. Philos Mag 1870;40:122.
- [33] Subramaniyan AK, Sun CT. Int J Solids Struct 2008;45:4340.
- [34] Zhou M. Proc R Soc A Math Phys Eng Sci 2003;459:2347.
- [35] Dommelen V. <http://eng.fsu.edu/~dommelen/papers/virial/index.pdf> 2003.
- [36] Wang J, Anderoglu O, Hirth JP, Misra a., Zhang X. Appl Phys Lett 2009;95:7.
- [37] Afanasyev KA, Sansoz F. Nano Lett 2007.
- [38] Yamakov V, Wolf D, Phillpot SR, Gleiter H. Acta Mater 2002;50:5005.
- [39] Wang J, Huang H. Appl Phys Lett 2004;85:5983.

- [40] Hu Q, Li L, Ghoniem NM. Acta Mater 2009;57:4866.
- [41] Wang J, Huang H. Appl Phys Lett 2006;88:203112.
- [42] Xu L, Xu D, Tu KN, Cai Y, Wang N, Dixit P, Pang JHL, Miao J. J Appl Phys 2008;104.
- [43] Wang J, Li N, Anderoglu O, Zhang X, Misra a., Huang JY, Hirth JP. Acta Mater 2010;58:2262.
- [44] Hirth,J.P., Lothe J. Theory of Dislocations, second ed. Malabar,FL:Krieger Pub.Co.; 1992.